# Testosterone acts through membrane protein GPRC6A to cause cardiac edema in zebrafish embryos

Vahid Zadmajid & Daniel A. Gorelick

Center for Precision Environmental Health
Department of Molecular & Cellular Biology
Baylor College of Medicine
One Baylor Plaza, BCM229
Houston, Texas 77030
USA

Correspondence to DAG: gorelick@bcm.edu

## Abstract

Androgen actions are classically thought to be mediated by intracellular androgen receptors (AR), but they can also exert non-genomic effects via binding to integral membrane proteins. Although several putative membrane androgen receptors were cloned and characterized *in vitro*, their function as androgen receptors *in vivo* remains to be further investigated. Here, we used a chemical-genetic screen in zebrafish and found that the G-protein coupled receptor GPRC6A mediates non-genomic androgen action during embryonic development. Exposure to three androgens, 5α-Androstane-3,17-dione (androstanedione), dihydrotestosterone (DHT), and testosterone, caused

cardiac edema or tail curvature in wild-type embryos. *ar* mutant embryos also exhibited cardiac edema or tail curvature following exposure to these androgens, suggesting the involvement of *ar*-independent pathways. To identify the causative receptor, we mutated putative membrane androgen receptors *gprc6a*, *hcar1-4*, or *zip9* genes and exposed mutant embryos to the androgens. We found that *hcar1-4* and *zip9* mutant embryos were susceptible to the identified androgens and developed cardiac edema or tail curvature phenotype following exposure. In contrast, we observed a significant reduction in cardiac edema phenotype in the *gprc6a* mutants compared to the wild-type embryos following testosterone treatment. Additionally, we exposed wild-type embryos to testosterone together with GPRC6A antagonists and observed a significant suppression of the cardiac edema phenotype. These results suggest that testosterone causes cardiac edema in zebrafish embryos by acting via the integral membrane protein GPRC6A, independently of nuclear androgen receptors. Overall, our study provides insights into non-genomic androgen signaling during embryonic development and identifies GPRC6A as a key receptor mediating androgen action.

## Introduction

Androgens regulate the development and function of multiple tissues and cell types, including muscle, heart, bone, skin, prostate, reproductive tract, and the brain (Bakker, 2022; Cunha et al., 2017; Murashima et al., 2015; Rossetti et al., 2017). Classically, androgens act by binding to cytosolic androgen receptors (AR), ligand-inducible transcription factors (Chang et al., 1988; Lubahn et al., 1988a; Lubahn et al., 1988b; Tilley et al., 1989; Trapman et al., 1988). Androgens can also activate signal transduction pathways independently of transcription, via a mechanism called non-genomic signaling (Gorczynska and Handelsman, 1995). These rapid androgen actions can be mediated by second messenger signaling pathways such as activation of intracellular kinases (eg MAPK, PI-3K) or increases in intracellular $Ca^{2+}$ (Estrada et al., 2003; Gatson and Singh, 2007; Gatson et al., 2006; Guo et al., 2002; Kang et al., 2004; Lieberherr and Grosse, 1994; Liu et al., 2022). Androgen signaling occurs in the absence of nuclear AR (Guo et al., 2002; Hatzoglou et al., 2005; Pi et al., 2010). Such non-genomic androgen signaling has been observed in different cell types, including T cells and macrophages (Benten et al., 1999; Wunderlich et al., 2002), osteoblasts (Kang et al., 2004; Lieberherr and Grosse, 1994), prostate and breast cancer cells (Hatzoglou et al., 2005; Liu et al., 2015; Sun et al., 2006), granulosa and Sertoli cells (Gorczynska and Handelsman, 1995; Machelon et al., 1998), and skeletal muscle (Estrada et al., 2000). However, the receptors that mediate non-genomic androgen signaling are not well understood.

Several putative membrane androgen receptors such as G protein-coupled receptor family C group 6 member A (GPRC6A) (Pi and Quarles, 2012; Pi et al., 2008;

68 Pi et al., 2010), the zinc transporter member 9 protein (ZIP9/SLC39A9) (Thomas et al.,
69 2014), the G protein-coupled oxo-eicosanoid receptor 1 (OXER1) (Kalyvianaki et al.,
70 2017), and ion channels such as transient receptor potential melastatin 8 (TRPM8)
71 (Asuthkar et al., 2015a; Asuthkar et al., 2015b), or L-type $Ca^{2+}$ channel, Cav1.2 (Scragg
72 et al., 2004; Scragg et al., 2007) were identified based on their ability to bind androgens
73 *in vitro*.

74 However, the evidence for androgen-dependent function of such proteins *in vivo*
75 is less clear, in part because receptors have multiple ligands. For example, zebrafish
76 *zip9* mutants exhibited reduced fecundity and egg viability compared with wild-type
77 (Converse and Thomas, 2020) while mouse and zebrafish with mutations in *Cav1.2*
78 exhibited cardiac abnormalities (Fu et al., 2011; Rosati et al., 2011; Rottbauer et al.,
79 2001; Seisenberger et al., 2000), but whether these phenotypes are influenced by
80 androgens, or other ligands binding to these receptors, is not known.

81 Here, we describe an *in vivo* screening approach combining chemical exposures
82 and CRISPR/Cas9 genome editing in zebrafish embryos to discover membrane
83 androgen receptors. Using this approach, we discovered that exposure to exogenous
84 testosterone alters cardiac development in zebrafish embryos, and that this occurs via
85 GPRC6A, independently of nuclear AR. We provide evidence that testosterone, and not
86 a metabolite, acts via GPRC6A. We also discovered that exposure to two additional
87 androgens, androstanedione and dihydrotestosterone, cause developmental
88 phenotypes in zebrafish, independently of nuclear AR, GPRC6A, ZIP9 or OXER1,
89 suggesting that additional membrane androgen receptors exist and influence embryonic
90 development.

91 **Materials and Methods**

92

93 **Zebrafish**

94 Zebrafish were raised at 28.5°C on a 14-h light, 10-h dark cycle in the Baylor College of
95 Medicine (BCM) Zebrafish Research Facility in a recirculating water system
96 (Aquaneering, Inc., San Diego, CA) and a Tecniplast recirculating water system
97 (Tecniplast USA, Inc., West Chester, PA). Wild-type zebrafish were AB strain
98 (Westerfield, 2000) and all mutant lines were generated on the AB strain. The following
99 previously published mutant lines were used: nuclear androgen receptor *ar* $^{uab142}$
100 (Crowder et al., 2018), estrogen receptor mutants *esr1a* $^{uab118}$ (ERα), *esr2a* $^{uab134}$
101 (ERβ1), and *esr2b* $^{uab128}$ (ERβ2) (Romano et al., 2017). All procedures were approved
102 by the BCM Institutional Animal Care and Use Committee.

103

104 **Embryo collection**

105 Adult zebrafish were allowed to spawn naturally in pairs or in groups. Embryos were
106 collected during 20 minute intervals to ensure precise developmental timing within a
107 group. Embryos were placed in 60 $cm^2$ Petri dishes at a density of no more than 100
108 per dish in E3B media (60X E3B: 17.2g NaCl, 0.76g KCl, 2.9g $CaCl_2$-$2H_2O$, 2.39g
109 $MgSO_4$ dissolved in 1 L Milli-Q water; diluted to 1X in 9 liter Milli-Q water plus 100 µL
110 0.02% methylene blue), and then stored in an incubator at 28.5°C on a 14-h light, 10-h
111 dark cycle. Between 24- and 48-hours post fertilization (hpf), embryos were manually
112 dechorionated.

113

114 **Embryo treatments**

115 At 2-4 hpf, embryos were incubated in E3B with androgen receptor modulator(s) or
116 estradiol at 28.5°C until imaging at 3 dpf. Dead embryos were removed daily. Embryos
117 that were alive but abnormal were left in the dish and recorded. All chemicals were
118 purchased as follows: androstanedione CAS registry number 846-46-8, Isosciences
119 catalog # 13386, purity ≥ 95%; dihydrotestosterone CAS 521-18-6, Isosciences catalog
120 # 6065UNL, purity ≥ 98%; testosterone CAS 58-22-0, Sigma catalog # T1500, purity ≥
121 98%; calindol CAS # 29610-18-8, Sigma catalog # SML1386, purity ≥ 98%; NPS-2143,
122 CAS # 324523-20-8, Sigma catalog # SML0362, purity ≥ 98%; epigallocatechin gallate,
123 CAS # 989-51-5, Sigma catalog # E4143, purity = 99.87%; estradiol, CAS # 50-28-2,
124 Sigma catalog # E8875, purity ≥ 98%. All chemical stocks were made in 100% DMSO at
125 1000x and diluted in E3B embryo media to the final concentration (1x) at the time of
126 treatment. All vehicle controls are 0.1% DMSO.

127

128 **CRISPR-Cas9 mutant generation**

129 Chemically synthesized gRNAs for *gprc6a*, *zip9*, *oxer1* (*hcar1-4*), *cav1.2*, and purified
130 Cas9 protein were obtained from Synthego (Redwood City, CA, USA). The target
131 sequences were identified using CHOPCHOP (Labun et al., 2021) or zebrafish genome-
132 scale lookup table from Wu et al. (Wu et al., 2018). Target site sequences are shown in
133 Table S1. 1-cell-stage embryos were injected using glass needles pulled on a Sutter
134 Instruments Fleming/Brown Micropipette Puller, model P-97, and a regulated air-
135 pressure micro-injector (Harvard Apparatus, New York, PL1–90). Each embryo was
136 injected with a 1 nl solution containing 1 µl of 10µM gRNA, 1 µl of 20µM Cas9 protein, 2

137 µl of 1.5 M KCl, 1 µl phenol red. The mixture was filled to 10 µL with 1X microinjection
138 buffer (10mM Tris-HCL, 0.1mM EDTA, pH 8.0 in nuclease-free $H_2O$) and incubated at
139 37 °C for 5-7 min before injection as described (Burger et al., 2016).
140
141 To generate *cyp19a1b* mutants, we hybridized oligonucleotides (oligo 1 5'-
142 TAGGAGCATGTGGTAAAGGATG, oligo 2 5'-AAACCATCCTTTACCACATGCT) to
143 generate double-stranded target DNA and annealed the DNA into digested pT7-gRNA
144 plasmid. pT7-gRNA plasmid was digested simultaneously with BsmBI, BglII and SalI for
145 one hour at 37 $^{o}$C followed by one hour at 55 $^{o}$C. gRNAs were synthesized and purified
146 from this plasmid template using in vitro transcription (MegaShortScript T7 kit, Life
147 Technologies). Cas9 mRNA was generated using in vitro transcription (mMessage
148 mMachine T3 kit, Life Technologies) from a linearized pT3TS-nCas9n plasmid. RNA
149 was purified using RNA clean & concentrator kit (Zymo Research). Plasmids pT7-gRNA
150 and pT3TS-nCas9n were obtained from Addgene (numbers 46759, 46757)(Jao et al.,
151 2013). Embryos were injected with a 1 nl solution containing 150 ng/µl of Cas9 mRNA,
152 50 ng/µl of gRNA and 0.1% phenol red.
153
154 For all gRNAs, mixtures were injected into the yolk of each embryo. Injected embryos
155 were raised to adulthood and crossed to wild-type fish (AB strain) to generate F1
156 embryos. F1 offspring were sequenced via tail fin biopsies to identify mutations
157 predicted to cause loss of functional protein.
158
159 **Genomic DNA isolation**

160 Individual embryos or tail biopsies from individual adults were placed in 100 µL ELB (10
161 mM Tris pH 8.3, 50 mM KCl, 0.3% Tween 20) with 1 µL proteinase K (800 U/ml, NEB) in
162 96 well plates, one sample per well. Samples were incubated at 55°C for 2 hours
163 (embryos) or 8 hours (tail clips) to extract genomic DNA. To inactivate Proteinase K,
164 plates were incubated at 98°C for 10 minutes and stored at -20°C.
165

166 **High resolution melt curve analysis**

167 PCR and melting curve analysis was performed as described (Parant et al., 2009). PCR
168 reactions contained 1 µl of LC Green Plus Melting Dye (BioFire Diagnostics), 1 µl of Ex
169 Taq Buffer, 0.8 µl of dNTP Mixture (2.5 mM each), 1 µl of each primer (5 µM), 0.05 µl of
170 Ex Taq (Takara Bio Inc), 1 µl of genomic DNA, and water up to 10 µl. PCR was
171 performed in a Bio-Rad C1000 Touch thermal cycler, using black/white 96 well plates
172 (Bio-Rad HSP9665). PCR reaction protocol was 98°C for 1 min, then 34 cycles of 98°C
173 for 10 sec, 60°C for 20 sec, and 72°C for 20 sec, followed by 72°C for 1 min. After the
174 final step, the plate was heated to 95°C for 20 sec and then rapidly cooled to 4°C.
175 Melting curves were generated with either a LightScanner HR 96 (Idaho Technology)
176 over a 70–95°C range and analyzed with LightScanner Instrument and Analysis
177 Software (V. 2.0.0.1331, Idaho Technology, Inc, Salt Lake City, UT), or with a Bio-Rad
178 CFX96 Real-Time System over a 70–95°C range and analyzed with Bio-Rad CFX
179 Manager 3.1 software. All mutations were confirmed by TA cloning and sequencing.
180 PCR primer sequences are shown in Table S2.
181

182 **Live imaging**

All embryos were imaged with a Nikon SMZ25 microscope equipped with a Hamamatsu ORCA-Flash4.0 digital CMOS camera, or with a Nikon SMZ18 microscope equipped with a Nikon DS-Fi3 camera. Images were equally adjusted for brightness and contrast in Adobe Photoshop CC 2022. For imaging of embryos following chemical exposure, embryos were imaged in E3B in 60 $mm^2$ dishes in 0.02% tricaine anesthetic. For embryos treated as mixed clutch, embryos were genotyped following imaging.

**Experimental design and data analysis**

Each experiment included comparing groups (treated vs untreated or mutant vs wildtype) using 11-160 embryos per group with all embryos from the same clutch. Experiments were performed on 3-6 clutches for each genotype. This is essentially a complete block design with clutch as block. Mean cardiac edema or tail curvature rate of individual embryos from a clutch was used for comparing treatment groups (or mutant groups) within experiments using one-way ANOVA with Tukey's multiple comparisons test. For some individual pairs of comparisons, paired t test was used. Significance level is 0.05. All Statistical analyses were performed using Prism version 9.4.1 (GraphPad Software, Boston, MA).

201 **Results**

202

203 **Strategy to identify membrane androgen receptors using genetic and**

204 **pharmacologic approaches**

205 The strategy we adopted is shown schematically in Figure 1. We exposed wild-type
206 embryos to multiple androgens at different concentrations (10-100 μM) in embryo
207 media, beginning at 3 hours post fertilization. We assayed embryo morphology at 2- and
208 3- days post fertilization (see Materials and Methods). We identified three androgens,
209 5α-Androstane-3,17-dione (androstanedione) (15 μM), dihydrotestosterone (DHT) (30
210 μM), and testosterone (30 μM), that caused a morphologic abnormality. All three
211 compounds caused cardiac edema with incompletely looped hearts (Figure 2, Table 1;
212 androstanedione mean embryos with cardiac edema 84% ± 12% standard deviation,
213 DHT 96% ± 6%, testosterone 79% ± 4%, n=6 clutches, 15-27 embryos per clutch).
214 Additionally, androstanedione and DHT, but not testosterone, caused a tail curvature
215 phenotype in which the caudal tail was curved dorsally (androstanedione mean
216 embryos with tail curvature 94% ± 5% standard deviation, DHT 81% ± 20). For embryos
217 exposed to androstanedione or DHT, every embryo that exhibited cardiac edema also
218 exhibited a tail curvature phenotype (Table 1). Other features of embryos, like gross
219 morphology of the head, eyes, somites, otolith, notochord, brain ventricles, fin folds, and
220 yolk, appeared normal, suggesting that these androgens affect specific developmental
221 processes and do not cause generalized, non-specific toxicity.

222

223 **Neither androstanedione, DHT, nor testosterone act via nuclear androgen**
224 **receptor (*ar*) to cause morphologic phenotypes in zebrafish embryos**
225 To explore whether these three androgens act via nuclear *ar* to cause morphologic
226 phenotypes, we crossed heterozygous *ar* $^{uab142/+}$ zebrafish to each other and exposed
227 the resulting embryos to vehicle (0.1% DMSO), androstanedione, DHT, or testosterone
228 beginning at 3 hours post fertilization. Following chemical exposure, we observed no
229 statistically significant difference in the percent of embryos exhibiting cardiac edema or
230 tail curvature phenotypes between wild-type, heterozygous *ar* $^{uab142/+}$, or homozygous *ar*
231 $^{uab142/uab142}$ embryos (Figure 2, Table 1). We conclude that zebrafish embryos with
232 mutations in nuclear *ar* are sensitive to androstanedione, DHT, or testosterone
233 exposure, which raises the possibility that these androgens act via an *ar*-independent
234 pathway to cause morphologic phenotypes during embryonic development.
235
236 **Testosterone, but not androstanedione or DHT, act via GPRC6A to cause cardiac**
237 **edema**
238 In the experiments described above, we showed that nuclear *ar* mutant embryos
239 remained sensitive to androstanedione, DHT, or testosterone exposure, suggesting the
240 involvement of *ar*-independent pathways. To determine whether these androgens act
241 via putative membrane androgen receptors, we took an F0 CRISPR genome editing
242 approach to generate zebrafish with mosaic mutations in putative membrane androgen
243 receptor genes: *gprc6a*, *zip9*, *oxer1* (*hcar1-4), cacna1c* (*cav1.2*) (Thomas, 2019;
244 Treviño and Gorelick, 2021)(Fig. S1). This approach enables us to inject embryos with a
245 cocktail of 4 guide RNAs together with Cas9 protein, targeting the same gene

246 redundantly, which induces mutations at a high enough burden to observe phenotypes
247 in the injected embryos (Hoshijima et al., 2019; Kroll et al., 2021; Wu et al., 2018).
248 We exposed embryos injected with gRNAs targeting *gprc6a*, *zip9*, *hcar1-4,*
249 *cacna1c*, or control embryos injected with Cas9 alone, to androstanedione, DHT,
250 testosterone or vehicle (0.1% DMSO) beginning at 3 hours post fertilization and
251 assayed morphology at 2- and 3-days post fertilization. Following androstanedione,
252 DHT, or testosterone exposure, *hcar1-4* and *zip9* mutant embryos exhibited cardiac
253 edema or tail curvature phenotype (Fig. 3). Untreated *cacna1c* mosaic mutant embryos
254 exhibited cardiac edema with abnormal heart morphology at 3 days post fertilization (not
255 shown). Therefore, we excluded *cacna1c* from further screening. Following chemical
256 exposure, we found no statistically significant difference in the proportion of embryos
257 with cardiac edema or tail curvature phenotype between control or *hcar1-4* and *zip9* F0
258 mosaic mutants (Fig 3, Table 2).
259 We found that *gprc6a* mosaic mutants had a statistically significant reduction in
260 the percent of embryos exhibiting cardiac edema following testosterone exposure
261 (Figure 3B, Table 3; embryos injected with Cas9 alone mean cardiac edema 65% ±
262 11%, *gprc6a* mosaic mutants 45% ± 9%, n=8 clutches, 42-164 embryos per clutch).
263 However, the *gprc6a* mosaic mutants remained sensitive to androstanedione or DHT
264 exposure (Fig. 3B, Table 2).
265 As an additional control, we injected wild-type embryos with Cas9 plus gRNAs
266 targeting an unrelated aryl hydrocarbon receptor gene *(ahr2)*. We exposed *ahr2* mosaic
267 mutant embryos to testosterone and assayed cardiac edema phenotype at 3 days post
268 fertilization. There was no statistically significant difference in the percent embryos

269 exhibiting cardiac edema between control embryos versus *ahr2* mosaic mutant embryos
270 (Fig. 3C, Table 2).
271 Our results suggest that testosterone causes cardiac edema by acting via the
272 integral membrane protein GPRC6A independently of nuclear androgen receptor. We
273 hypothesize that GPRC6A acts as a membrane receptor for testosterone in zebrafish
274 embryos. This is consistent with results from cultured cells and adult mouse tissues
275 suggesting that *Gprc6a* responds to testosterone (Pi et al., 2010; Pi et al., 2015).
276
277 **CRISPR–Cas9 mutagenesis efficiency in F0 embryos**
278 The absence of a phenotype in a CRISPR screen could be due to low efficiency of
279 gRNAs. It is possible that targeting *zip9* or *hcar1-4* failed to rescue androgen
280 phenotypes because the *zip9* and *hcar1-4* gRNAs had low efficacy. To evaluate the
281 mutagenesis efficiency in our F0 embryos, we isolated genomic DNA from individual
282 embryos at 24 hours post fertilization. The targeted site was amplified using PCR.
283 Amplicons were Sanger sequenced and then deconvoluted and analyzed using the ICE
284 (Inference of CRISPR Edits) algorithm(Conant et al., 2022). We compared indel
285 mutations (the percent of sequence from each embryo that has a mutation) or knockout
286 score (the percent of mutations from each embryo that were predicted to produce a
287 non-functional protein) for each gRNA (Fig. S2). Different guides acted with variable
288 effectiveness. In the cocktail of 4 guide RNA sets to target *gprc6a*, G4 produced an
289 average of more than 50% indel mutations or knockout score (n=38 embryos from 2
290 clutches). G1 and G2 were less effective, with an average mutation frequency of less

291 than 10% (n=40 embryos from 2 clutches), and G3 produced 0% mutation (n=38
292 embryos from 2 clutches) (Fig. S2).
293 Comparing the efficiency of guide RNAs targeting *zip9*, G1, and G3 were the
294 most effective. G1 induced an average of 78% indel mutations (n=40 embryos from 2
295 clutches) or 52% knockout score (n=40 embryos from 2 clutches), and G3 induced an
296 average of 73% indel mutations (n=45 embryos from 2 clutches) or 5% knockout score
297 (n=45 embryos from 2 clutches). For *hcar1-4*, the average indel mutations or knockout
298 score for all G1, G2, and G4 was greater than 50% (n=2 clutches/24-45 embryos per
299 clutch). In analyzed *hcar1-4* mosaic mutant embryos, G4 induced greater than 90%
300 indel mutations or knockout-score (n=46 embryos from 2 clutches). Overall, these
301 results confirm the efficacy of multi-locus targeting to generate zebrafish F0 mutants for
302 the purpose of initial screening of gene function.
303
304 **Zygotic *gprc6a* mutants recapitulate phenotypes observed in mosaic mutants**
305 To validate our observations, we generated heritable, non-mosaic mutations in
306 *gprc6a* and determined whether homozygous embryos were protected from
307 testosterone-dependent cardiac edema, as were F0 mosaic mutants. We injected wild-
308 type embryos with Cas9 together with the same set of 4 guide RNAs, targeting different
309 coding regions of the *gprc6a* gene, as we did to generate *gprc6a* mosaic mutants (Fig.
310 S3). Injected embryos were raised to adulthood and outcrossed to wild-type zebrafish to
311 generate heterozygous F1 embryos. Heterozygous F1 adult fish were sequenced to
312 identify mutations predicted to cause loss of functional GPRC6A protein. We identified
313 several mutant alleles in F1 fish and derived five independent *gprc6a* mutant lines, from

314 which we performed experiments on homozygous embryos: *gprc6a* $^{bcm53/-;\ bcm52/-}$, *gprc6a*
315 $^{bcm56/-;\ bcm54/-;\ bcm55/-}$, *gprc6a* $^{bcm56/-;\ bcm54/-}$, *gprc6a* $^{bcm59/-;\ bcm58/-}$, and *gprc6a* $^{bcm61/-;\ bcm60/-}$
316 (Fig. S3A). For example, *bcm53* is a 1 bp deletion in exon 1 resulting in a frameshift at
317 amino acid 44 and a premature stop codon at amino acid 50 in the ligand binding
318 domain. *bcm5*2 is a 1 bp deletion in exon 3 resulting in a frameshift at amino acid 225
319 and a premature stop codon at amino acid 250. These two alleles are genetically linked
320 (we were unable to generate fish containing *bcm52* without *bcm53*), however the
321 upstream allele (*bcm53*) is likely driving the loss of function. We did not observe any
322 morphologic differences among untreated *gprc6a* $^{bcm53/-;\ bcm52/-}$, *gprc6a* $^{bcm56/-;\ bcm54/-;}$
323 $^{bcm55/-}$, *gprc6a* $^{bcm56/-;\ bcm54/-}$, *gprc6a* $^{bcm59/-;\ bcm58/-}$, and *gprc6a* $^{bcm61/-;\ bcm60/-}$ embryos.
324 We exposed homozygous *gprc6a* embryos to vehicle, androstanedione, DHT, or
325 testosterone beginning at 3 hours post fertilization. Each clutch contained a mix of wild-
326 type and mutant embryos (denoted as wild-type +/+, heterozygous +/-, or homozygous -
327 /-; Fig 4A). Following testosterone exposure, homozygous *gprc6a* mutant embryos
328 exhibited partial cardiac edema rescue, similar to what we observed in mosaic F0
329 mutants (Figure 4B, Table 3; wild-type mean percent cardiac edema 76% ± 9%,
330 heterozygous 76% ± 8%, homozygous 58% ± 10%, n=13 clutches, 12-57 embryos per
331 clutch). Analyzing the response of each allele separately revealed similar results (Fig.
332 S4, Table 3). Homozygous *gprc6a* mutants remained sensitive to androstanedione and
333 DHT exposure, similar to wild-type embryos (Fig. 4B, Table 3). We conclude that the F0
334 CRISPR *gprc6a* mosaic mutants recapitulate what occurs in non-mosaic homozygous
335 mutants. Taken together, our results suggest that testosterone causes cardiac edema
336 by acting via the integral membrane protein GPRC6A independently of the nuclear *ar*.

337

338 **GPRC6A antagonists inhibit testosterone-dependent cardiac edema in wild-type**
339 **embryos**

340 To further confirm that testosterone acts through *gprc6a* to cause cardiac edema,
341 we tested whether GPRC6A antagonists block testosterone-driven cardiac edema. We
342 exposed wild-type embryos to testosterone together with different GPRC6A antagonists,
343 NPS-2143 (5 μM), calindol (5 μM), and epigallocatechin gallate (EGCG, 100 μM) at
344 concentrations used to study GPRC6A responses in cultured cells (Faure et al., 2009;
345 Mizuta et al., 2021; Pi et al., 2018). We confirmed that 5 μM NPS-2143, 5 μM calindol,
346 and 100 μM EGCG do not cause abnormalities in embryos in the absence of androgen
347 exposure (Fig. 5A, Table 4). We found that wild-type embryos exposed to NPS-2143 or
348 EGCG with testosterone had statistically significantly reduced cardiac edema compared
349 to embryos exposed to testosterone alone (Figure 5A, Table 4; testosterone mean
350 embryos with cardiac edema 69% ± 7%, testosterone + NPS-2143 39% ± 9%,
351 testosterone + EGCG 32% ± 8%, n=6 clutches, 43-63 embryos per clutch). While NPS-
352 2143 and EGCG partially blocked testosterone-driven cardiac edema, calindol failed to
353 reduce testosterone-dependent cardiac edema (Fig. 5A, Table 4). Calindol was
354 developed as a calcimimetic that binds the human calcium sensing receptor and has
355 lower selectivity towards GPRC6A (Gloriam et al., 2011; Kessler et al., 2004). The
356 failure of calindol to inhibit zebrafish GPRC6A could be due to the lower selectivity
357 together with differences between zebrafish and human GPRC6A proteins.

358 To test whether NPS-2143 and EGCG act specifically on zebrafish GPRC6A, we
359 exposed homozygous *gprc6a* mutant embryos to testosterone alone or together with

360 NPS-2143 and EGCG and assayed cardiac edema. There was no statistically
361 significant difference in the percent of *gprc6a* homozygous embryos exhibiting cardiac
362 edema following exposure to NPS-2143 or EGCG alone or in combination with
363 testosterone (Figure 5B, Table 4; testosterone mean embryos with cardiac edema 45%
364 ± 5%, testosterone + NPS-2143 55% ± 5%, testosterone + EGCG 47% ± 6%, n=4
365 clutches, 18-30 embryos per clutch). These results show that the zebrafish *gprc6a*
366 mutants do not respond to GPRC6A antagonists and supports the hypothesis that
367 testosterone acts via GPRC6A to cause cardiac edema.
368

369 **Testosterone, and not a metabolite, causes cardiac edema in a GPRC6A-**
370 **dependent manner**

371 Testosterone is metabolized into molecules like estradiol. We showed that exposure to
372 testosterone caused cardiac edema in a GPRC6A-dependent manner. However, it is
373 not known whether testosterone, or a metabolite, is the active compound that causes
374 the phenotype. We hypothesize that testosterone itself acts on GPRC6A to cause
375 cardiac edema in zebrafish embryos. To test whether estradiol, a testosterone
376 metabolite, causes a phenotype similar to testosterone, we exposed wild-type embryos
377 at 3 hours post fertilization to 30 μM estradiol or 30 μM testosterone and assayed
378 morphologic phenotypes at 3 days post fertilization. We found that exposure of wild-type
379 embryos to estradiol did not cause cardiac edema or other morphologic phenotypes
380 (Fig. 6A, Table 5), supporting the hypothesis that testosterone, and not estradiol, is the
381 active compound that causes the phenotype.

382 To further test whether testosterone acts on GPRC6A directly *in vivo*, we
383 generated aromatase mutant embryos and asked whether testosterone causes a
384 phenotype in an aromatase-dependent manner. Aromatase is the rate-limiting enzyme
385 in the conversion of testosterone into estradiol (Conley and Hinshelwood, 2001; Duffy et
386 al., 2010). Zebrafish have two aromatase genes, *cyp19a1a* and *cyp19a1b* (Chiang et
387 al., 2001a; Chiang et al., 2001b). *cyp19a1a* is expressed exclusively in the gonads
388 (which do not begin developing until ~10 days post fertilization), while *cyp19a1b* is
389 expressed in the brain at 2 days post fertilization (Chiang et al., 2001a; Chiang et al.,
390 2001b; Lassiter and Linney, 2007). Here we focused on the *cyp19a1b* gene because of
391 its expression during embryonic development.
392 Using CRISPR/Cas9, we generated heritable mutant alleles for *cyp19a1b* with a
393 20 bp insertion in exon 2 (Fig. S5A, maternal zygotic *cyp19a1b* mutant *MZcyp19a1b*
394 $^{uab124}$). The mutation is predicted to result in a frameshift at amino acid 11 and a
395 premature stop codon at amino acid 30 (Fig. S5B). We exposed *MZcyp19a1b* $^{uab124}$
396 embryos to vehicle (0.1% DMSO) or testosterone at 3 hours post fertilization and
397 assayed morphologic phenotypes at 3 days post fertilization. *MZcyp19a1b* $^{uab124}$
398 embryos remained sensitive to testosterone exposure, similar to what we observed
399 when wild-type embryos were exposed to testosterone (Figure 6B, Table 5; wild-type
400 mean embryos cardiac edema 85% ± 8%, *MZcyp19a1b* 82% ± 6%, n=4 clutches, 21-35
401 embryos per clutch). These results suggest that aromatase is not required for
402 testosterone-dependent cardiac edema.
403 To exclude the possibility that testosterone acts via estrogen receptors (either via
404 non-specific binding or via crosstalk between GPRC6A and nuclear estrogen receptors),

405 we exposed estrogen receptor mutant embryos, *esr1a* $^{uab118/-}$ (ERα), *esr2a* $^{uab134/-}$
406 (ERβ1), and *esr2b* $^{uab128/-}$ (ERβ2) to testosterone. We found no significant difference in
407 the percent of embryos exhibiting cardiac edema phenotype between wild-type or
408 heterozygous embryos versus homozygous *esr1a* $^{uab118/-}$, *esr2a* $^{uab134/-}$, and *esr2b* $^{uab128/-}$
409 mutant embryos after testosterone exposure (Figure 6C-E, Table 5). Taken together,
410 these results suggest that testosterone, and not a metabolite, is the active agent that
411 causes cardiac edema via GPRC6A.
412
413

414 **Discussion**

415 We demonstrate that a CRISPR screen in zebrafish embryos can be used to
416 identify genes required for testosterone-dependent phenotypes. The zebrafish
417 screening approach complements existing cell-based approaches. Membrane steroid
418 receptors are typically identified based on their binding or activity in cultured cells, and
419 then tested for similar activity *in vivo*. It can be difficult to determine whether a receptor
420 responds to steroids *in vivo*, especially receptors that have multiple ligands. For
421 example, the estrogen receptor modulator tamoxifen was shown to bind directly to the
422 human sodium channel Nav1.2 and inhibit sodium conductance *in vitro* (Sula et al.,
423 2021), but whether this occurs *in vivo* is not known. The zebrafish screening approach
424 allows for the direct identification of membrane steroid receptors *in vivo*.

425 Our approach relies on using CRISPR-Cas9 to rapidly generate mutant
426 zebrafish. To generate heritable mutants, germline transmitting animals need to be
427 identified and mated to produce homozygous embryos, a process that takes months. In
428 contrast, analyzing gene function in mosaic mutant animals (F0 generation) takes less
429 than a week. Our approach was enabled by recent findings that injecting zebrafish
430 embryos with Cas9 protein and a cocktail of 3-4 guide RNAs targeting the same gene
431 induces mutations at a high enough burden to observe phenotypes in mosaic mutant
432 embryos (Klatt Shaw and Mokalled, 2021; Kroll et al., 2021; Wu et al., 2018). One
433 potential limitation of CRISPR screens is the failure of F0 mosaic mutants to
434 recapitulate phenotypes found in heritable, non-mosaic mutants (eg F1 and subsequent
435 generations). In our screen, this was not the case. We identified similar phenotypes in

436 F0 mosaic and in non-mosaic *gprc6a* mutants (compare figures 3 and 4), demonstrating
437 the validity of using the F0 CRISPR screening approach.

438 Our pilot screen tested 4 candidate genes using CRISPR-Cas9. However, new
439 barcoding and microfluidics approaches, such as MIC-Drop, could allow us to screen
440 and mutate hundreds or thousands of genes (Parvez et al., 2021). Combining different
441 chemical exposures with MIC-Drop offers the unprecedented ability to comprehensively
442 identify membrane receptors for any steroid molecule that causes a phenotype in
443 zebrafish embryos. Here, we assayed gross, easily observable morphologic
444 phenotypes. It is also possible to assay more subtle phenotypes, for example by using
445 transgenic reporter zebrafish that mark a cell-type of interest, or by using assays to
446 measure behaviors like locomotor activity.

447 Our chemical-genetic F0 CRISPR screening approach has several limitations.
448 Our scheme relies on identifying phenotypes following exposure to steroids, and then
449 testing whether a gene mutation rescues the exposure phenotype (Figure 1). If a mutant
450 has a phenotype in the absence of chemical exposure, then we cannot test that gene.
451 For example, embryos injected with gRNAs targeting *cav1.2* exhibited cardiac edema in
452 the absence of chemical exposure. Consequently, we could not test whether *cav1.2*
453 mutations rescue testosterone-dependent cardiac edema. This also demonstrates the
454 strength of the approach. The phenotype we observed in *cav1.2* mosaic mutants was
455 similar to the phenotypes observed in *cav1.2* heritable, homozygous mutants (Rottbauer
456 et al., 2001), further supporting the idea that F0 mosaic mutants recapitulate
457 phenotypes observed in heritable, non-mosaic mutants.

458 Another limitation is that genetic compensation could produce false negative
459 results. A mutation in a gene could lead to upregulation of a related gene that
460 compensates for the original mutation. In this case, we would falsely conclude that the
461 target gene is not involved in steroid signaling. Future studies can overcome this
462 limitation by performing a deletion screen, using two gRNAs flanking the target gene to
463 delete the entire target gene. This would prevent production of mRNA and consequently
464 would reduce the occurrence of compensation triggered by mutant mRNA (El-Brolosy et
465 al., 2019; Fernandez-Abascal et al., 2022; Ma et al., 2019; Serobyan et al., 2020).
466 Another concern are phenotypes resulting from the off-target effects of Cas9. These can
467 be validated by performing RNA rescue studies or by generating heritable, non-mosaic
468 mutations in the target gene. By successively breeding such mutants with wild-type
469 animals, one selects for the target mutation and loses potential off-target mutations.
470 This is the strategy we employed. We found that homozygous *gprc6a* mutants are
471 partially resistant to testosterone exposure (Figure 4), similar to what we observed in
472 mosaic *gprc6a* F0 mutants (Figure 3). Thus, the off-target effects of Cas9 are unlikely to
473 influence our results.
474 We found that testosterone exposure caused cardiac edema and heart
475 malformations in approximately 80% of wild-type embryos. This phenotype was partially
476 rescued by co-administration of two different GPRC6A antagonists (Figure 5). The
477 testosterone phenotype was also partially rescued in *gprc6a* mutants (both mosaic F0
478 and heritable homozygotes, Figure 3, Figure 4). Similar results using F0 mosaic and
479 non-mosaic mutants, and using pharmacologic antagonists, suggests the partial rescue
480 is not an artifact of mutagenesis. What explains the lack of a complete rescue?

481 Testosterone could be acting simultaneously through multiple receptors, in addition to
482 GPRC6A, to cause cardiac abnormalities. *ar uab142* mutants remained sensitive to
483 testosterone exposure, suggesting that testosterone acts independently of nuclear AR
484 here. We cannot exclude the possibility that *uab142* mutants are hypomorphs that retain
485 partial function of AR. Thus, it is possible that testosterone causes cardiac edema by
486 acting through both GPRC6A and nuclear AR. Testing *gprc6a;ar* double mutants, or
487 generating *ar* deletion mutants, could answer this question more directly. Testosterone
488 could also be acting simultaneously through multiple pathways, for example by binding
489 to receptors and by altering the fluidity of cell membranes or the mobility of membrane
490 proteins (Liang et al., 2001; Shivaji and Jagannadham, 1992; Whiting et al., 1995;
491 Whiting et al., 2000).

492 Our results are the first to identify a role for androgen-dependent GPRC6A
493 activity during embryonic development. Our results are consistent with results from
494 cultured cells and mouse models demonstrating that GPRC6A responds to
495 testosterone. In HEK-293 cells, testosterone stimulated extracellular signal-regulated
496 kinase (ERK) activity, which was blocked by GPRC6A antagonists (Pi et al., 2018). In
497 wild-type mice, testosterone treatment increased levels of phosphorylated ERK and
498 Egr-1 expression in bone marrow and testis, which was reduced or absent in GPRC6A
499 mutant mice (Pi et al., 2010). Several ligands activate GPRC6A, including calcium,
500 magnesium, and the peptide hormone osteocalcin (Pi et al., 2005). It remains to be seen
501 whether or how testosterone influences the response of GPRC6A to other ligands.
502 Osteocalcin is maternally deposited into zebrafish oocytes and expressed at 2 days
503 post fertilization (Bensimon-Brito et al., 2012), developmental stages when embryos

504 exposed to testosterone exhibit cardiac phenotypes. Future studies could explore
505 whether osteocalcin is required for testosterone-GPRC6A-dependent cardiac
506 phenotypes.

507 In conclusion, we developed a combined chemical and genetic screening
508 approach to identify genes required for androgen-dependent phenotypes in zebrafish
509 embryos. Our pilot screen revealed that testosterone acts via GPRC6A to cause cardiac
510 phenotypes. This chemical-genetic screening platform can be adapted to discover
511 genes encoding membrane proteins that act as receptors for any steroid or related
512 small molecule.

513

514 **Acknowledgements**

515 We thank Lauren Pandolfo and the staff of the BCM zebrafish facility for caring for our
516 zebrafish, the members of NR IMPACT for scientific feedback during the early phases
517 of this project, and members of the Gorelick laboratory for advice on experiments. This
518 work was supported by the training program in Precision Environmental Health
519 Sciences T32 ES027801.

520

521 **References**

522 **Asuthkar, S., Elustondo, P. A., Demirkhanyan, L., Sun, X., Baskaran, P., Velpula,**
523 **K. K., Thyagarajan, B., Pavlov, E. V. and Zakharian, E.** (2015a). The TRPM8
524 protein is a testosterone receptor: I. Biochemical evidence for direct TRPM8-
525 testosterone interactions. *J. Biol. Chem.* **290**, 2659–2669.

526 **Asuthkar, S., Demirkhanyan, L., Sun, X., Elustondo, P. A., Krishnan, V., Baskaran,**
527 **P., Velpula, K. K., Thyagarajan, B., Pavlov, E. V. and Zakharian, E.** (2015b). The
528 TRPM8 protein is a testosterone receptor: II. Functional evidence for an ionotropic
529 effect of testosterone on TRPM8. *J. Biol. Chem.* **290**, 2670–2688.

530 **Bakker, J.** (2022). The role of steroid hormones in the sexual differentiation of the
531 human brain. *J. Neuroendocrinol.* **34**, e13050.

532 **Bensimon-Brito, A., Cardeira, J., Cancela, M. L., Huysseune, A. and Witten, P. E.**
533 (2012). Distinct patterns of notochord mineralization in zebrafish coincide with the
534 localization of Osteocalcin isoform 1 during early vertebral centra formation. *BMC*
535 *Dev. Biol.* **12**, 28.

536 **Benten, W. P., Lieberherr, M., Stamm, O., Wrehlke, C., Guo, Z. and Wunderlich, F.**
537 (1999). Testosterone signaling through internalizable surface receptors in androgen
538 receptor-free macrophages. *Mol. Biol. Cell* **10**, 3113–3123.

539 **Burger, A., Lindsay, H., Felker, A., Hess, C., Anders, C., Chiavacci, E., Zaugg, J.,**
540 **Weber, L. M., Catena, R., Jinek, M., et al.** (2016). Maximizing mutagenesis with

541 solubilized CRISPR-Cas9 ribonucleoprotein complexes. *Development* **143**, 2025–
542 2037.

543 **Chang, C. S., Kokontis, J. and Liao, S. T.** (1988). Molecular cloning of human and rat
544 complementary DNA encoding androgen receptors. *Science* **240**, 324–326.

545 **Chiang, E. F., Yan, Y. L., Guiguen, Y., Postlethwait, J. and Chung Bc** (2001a). Two
546 Cyp19 (P450 aromatase) genes on duplicated zebrafish chromosomes are expressed
547 in ovary or brain. *Mol. Biol. Evol.* **18**, 542–550.

548 **Chiang, E. F., Yan, Y. L., Tong, S. K., Hsiao, P. H., Guiguen, Y., Postlethwait, J. and**
549 **Chung, B. C.** (2001b). Characterization of duplicated zebrafish cyp19 genes. *J. Exp.*
550 *Zool.* **290**, 709–714.

551 **Conant, D., Hsiau, T., Rossi, N., Oki, J., Maures, T., Waite, K., Yang, J., Joshi, S.,**
552 **Kelso, R., Holden, K., et al.** (2022). Inference of CRISPR Edits from Sanger Trace
553 Data. *The CRISPR Journal* **5**, 123–130.

554 **Conley, A. and Hinshelwood, M.** (2001). Mammalian aromatases. *Reproduction* **121**,
555 685–695.

556 **Converse, A. and Thomas, P.** (2020). The zinc transporter ZIP9 (Slc39a9) regulates
557 zinc dynamics essential to egg activation in zebrafish. *Sci. Rep.* **10**, 15673.

558 **Crowder, C. M., Lassiter, C. S. and Gorelick, D. A.** (2018). Nuclear androgen receptor
559 regulates testes organization and oocyte maturation in zebrafish. *Endocrinology* **159**,
560 980–993.

561 **Cunha, G. R., Kurita, T., Cao, M., Shen, J., Robboy, S. and Baskin, L.** (2017).
562 Molecular mechanisms of development of the human fetal female reproductive tract.
563 *Differentiation.* **97**, 54–72.

564 **Duffy, T. A., Picha, M. E., Won, E. T., Borski, R. J., McElroy, A. E. and Conover, D.**
565 **O.** (2010). Ontogenesis of gonadal aromatase gene expression in atlantic silverside
566 (Menidia menidia) populations with genetic and temperature-dependent sex
567 determination. *J. Exp. Zool. A Ecol. Genet. Physiol.* **313**, 421–431.

568 **El-Brolosy, M. A., Kontarakis, Z., Rossi, A., Kuenne, C., Günther, S., Fukuda, N.,**
569 **Kikhi, K., Boezio, G. L. M., Takacs, C. M., Lai, S.-L., et al.** (2019). Genetic
570 compensation triggered by mutant mRNA degradation. *Nature* **568**, 193–197.

571 **Estrada, M., Liberona, J. L., Miranda, M. and Jaimovich, E.** (2000). Aldosterone- and
572 testosterone-mediated intracellular calcium response in skeletal muscle cell cultures.
573 *Am. J. Physiol. Endocrinol. Metab.* **279**, E132-9.

574 **Estrada, M., Espinosa, A., Müller, M. and Jaimovich, E.** (2003). Testosterone
575 stimulates intracellular calcium release and mitogen-activated protein kinases via a G
576 protein-coupled receptor in skeletal muscle cells. *Endocrinology* **144**, 3586–3597.

577 **Faure, H., Gorojankina, T., Rice, N., Dauban, P., Dodd, R. H., Bräuner-Osborne, H.,**
578 **Rognan, D. and Ruat, M.** (2009). Molecular determinants of non-competitive
579 antagonist binding to the mouse GPRC6A receptor. *Cell Calcium* **46**, 323–332.

580 **Fernandez-Abascal, J., Wang, L., Graziano, B., Johnson, C. K. and Bianchi, L.**
581 (2022). Exon-dependent transcriptional adaptation by exon-junction complex proteins
582 Y14/RNP-4 and MAGOH/MAG-1 in Caenorhabditis elegans. *PLoS Genet.* **18**,
583 e1010488.

584 **Fu, Y., Westenbroek, R. E., Yu, F. H., Clark, J. P., Marshall, M. R., Scheuer, T. and**
585 **Catterall, W. A.** (2011). Deletion of the distal C terminus of CaV1.2 channels leads to
586 loss of beta-adrenergic regulation and heart failure in vivo. *J. Biol. Chem.* **286**, 12617–
587 12626.

588 **Gatson, J. W. and Singh, M.** (2007). Activation of a membrane-associated androgen
589 receptor promotes cell death in primary cortical astrocytes. *Endocrinology* **148**, 2458–
590 2464.

591 **Gatson, J. W., Kaur, P. and Singh, M.** (2006). Dihydrotestosterone differentially
592 modulates the mitogen-activated protein kinase and the phosphoinositide 3-
593 kinase/Akt pathways through the nuclear and novel membrane androgen receptor in
594 C6 cells. *Endocrinology* **147**, 2028–2034.

595 **Gloriam, D. E., Wellendorph, P., Johansen, L. D., Thomsen, A. R. B., Phonekeo, K.,**
596 **Pedersen, D. S. and Bräuner-Osborne, H.** (2011). Chemogenomic discovery of
597 allosteric antagonists at the GPRC6A receptor. *Chem. Biol.* **18**, 1489–1498.

598 **Gorczynska, E. and Handelsman, D. J.** (1995). Androgens rapidly increase the
599 cytosolic calcium concentration in Sertoli cells. *Endocrinology* **136**, 2052–2059.

600 **Guo, Z., Benten, W. P. M., Krücken, J. and Wunderlich, F.** (2002). Nongenomic
601 testosterone calcium signaling. Genotropic actions in androgen receptor-free
602 macrophages. *J. Biol. Chem.* **277**, 29600–29607.

603 **Hatzoglou, A., Kampa, M., Kogia, C., Charalampopoulos, I., Theodoropoulos, P.**
604 **A., Anezinis, P., Dambaki, C., Papakonstanti, E. A., Stathopoulos, E. N.,**
605 **Stournaras, C., et al.** (2005). Membrane androgen receptor activation induces
606 apoptotic regression of human prostate cancer cells in vitro and in vivo. *J. Clin.*
607 *Endocrinol. Metab.* **90**, 893–903.

608 **Hoshijima, K., Jurynec, M. J., Klatt Shaw, D., Jacobi, A. M., Behlke, M. A. and**
609 **Grunwald, D. J.** (2019). Highly Efficient CRISPR-Cas9-Based Methods for
610 Generating Deletion Mutations and F0 Embryos that Lack Gene Function in Zebrafish.
611 *Dev. Cell* **51**, 645-657.e4.

612 **Jao, L.-E., Wente, S. R. and Chen, W.** (2013). Efficient multiplex biallelic zebrafish
613 genome editing using a CRISPR nuclease system. *Proc Natl Acad Sci USA* **110**,
614 13904–13909.

615 **Kalyvianaki, K., Gebhart, V., Peroulis, N., Panagiotopoulou, C., Kiagiadaki, F.,**
616 **Pediaditakis, I., Aivaliotis, M., Moustou, E., Tzardi, M., Notas, G., et al.** (2017).
617 Antagonizing effects of membrane-acting androgens on the eicosanoid receptor
618 OXER1 in prostate cancer. *Sci. Rep.* **7**, 44418.

619 **Kang, H.-Y., Cho, C.-L., Huang, K.-L., Wang, J.-C., Hu, Y.-C., Lin, H.-K., Chang, C.**
620 **and Huang, K.-E.** (2004). Nongenomic androgen activation of phosphatidylinositol 3-

621 kinase/Akt signaling pathway in MC3T3-E1 osteoblasts. *J. Bone Miner. Res.* **19**,
622 1181–1190.

623 **Kessler, A., Faure, H., Petrel, C., Ruat, M., Dauban, P. and Dodd, R. H.** (2004). N2-
624 benzyl-N1-(1-(1-naphthyl)ethyl)-3-phenylpropane-1,2-diamines and conformationally
625 restrained indole analogues: development of calindol as a new calcimimetic acting at
626 the calcium sensing receptor. *Bioorg. Med. Chem. Lett.* **14**, 3345–3349.

627 **Klatt Shaw, D. and Mokalled, M. H.** (2021). Efficient CRISPR/Cas9 mutagenesis for
628 neurobehavioral screening in adult zebrafish. *G3 (Bethesda)* **11**,.

629 **Kroll, F., Powell, G. T., Ghosh, M., Gestri, G., Antinucci, P., Hearn, T. J., Tunbak,**
630 **H., Lim, S., Dennis, H. W., Fernandez, J. M., et al.** (2021). A simple and effective F0
631 knockout method for rapid screening of behaviour and other complex phenotypes.
632 *eLife* **10**,.

633 **Labun, K., Krause, M., Torres Cleuren, Y. and Valen, E.** (2021). CRISPR genome
634 editing made easy through the CHOPCHOP website. *Curr. Protoc.* **1**, e46.

635 **Lassiter, C. S. and Linney, E.** (2007). Embryonic expression and steroid regulation of
636 brain aromatase cyp19a1b in zebrafish (Danio rerio). *Zebrafish* **4**, 49–57.

637 **Liang, Y., Belford, S., Tang, F., Prokai, L., Simpkins, J. W. and Hughes, J. A.**
638 (2001). Membrane fluidity effects of estratrienes. *Brain Res. Bull.* **54**, 661–668.

639 **Lieberherr, M. and Grosse, B.** (1994). Androgens increase intracellular calcium
640 concentration and inositol 1,4,5-trisphosphate and diacylglycerol formation via a
641 pertussis toxin-sensitive G-protein. *J. Biol. Chem.* **269**, 7217–7223.

642 **Liu, G., Honisch, S., Liu, G., Schmidt, S., Alkahtani, S., AlKahtane, A. A.,**
643 **Stournaras, C. and Lang, F.** (2015). Up-regulation of Orai1 expression and store
644 operated Ca(2+) entry following activation of membrane androgen receptors in MCF-7
645 breast tumor cells. *BMC Cancer* **15**, 995.

646 **Liu, G., Han, S., Jiang, S., Jiang, Y., Chen, C., Sun, N. and Che, H.** (2022).
647 Extracellular Ca2+ aggravates IgE-induced allergic reaction in mast cells through
648 GPRC6A, a novel family C G-protein-coupled receptor. *Life Sci.* **311**, 121013.

649 **Lubahn, D. B., Joseph, D. R., Sullivan, P. M., Willard, H. F., French, F. S. and**
650 **Wilson, E. M.** (1988a). Cloning of human androgen receptor complementary DNA
651 and localization to the X chromosome. *Science* **240**, 327–330.

652 **Lubahn, D. B., Joseph, D. R., Sar, M., Tan, J., Higgs, H. N., Larson, R. E., French,**
653 **F. S. and Wilson, E. M.** (1988b). The human androgen receptor: complementary
654 deoxyribonucleic acid cloning, sequence analysis and gene expression in prostate.
655 *Mol. Endocrinol.* **2**, 1265–1275.

656 **Machelon, V., Nomé, F. and Tesarik, J.** (1998). Nongenomic effects of
657 androstenedione on human granulosa luteinizing cells. *J. Clin. Endocrinol. Metab.* **83**,
658 263–269.

659 **Ma, Z., Zhu, P., Shi, H., Guo, L., Zhang, Q., Chen, Y., Chen, S., Zhang, Z., Peng, J.**
660 **and Chen, J.** (2019). PTC-bearing mRNA elicits a genetic compensation response
661 via Upf3a and COMPASS components. *Nature* **568**, 259–263.

662 **Mizuta, H., Kumamoto, N., Ugawa, S. and Yamamoto, T.** (2021). Additive Effects of
663 L-Ornithine on Preferences to Basic Taste Solutions in Mice. *Nutrients* **13**,.

664 **Murashima, A., Kishigami, S., Thomson, A. and Yamada, G.** (2015). Androgens and
665 mammalian male reproductive tract development. *Biochim. Biophys. Acta* **1849**, 163–
666 170.

667 **Parant, J. M., George, S. A., Pryor, R., Wittwer, C. T. and Yost, H. J.** (2009). A rapid
668 and efficient method of genotyping zebrafish mutants. *Dev. Dyn.* **238**, 3168–3174.

669 **Parvez, S., Herdman, C., Beerens, M., Chakraborti, K., Harmer, Z. P., Yeh, J. J.,**
670 **MacRae, C. A., Yost, H. J. and Peterson, R. T.** (2021). MIC-Drop: A platform for
671 large-scale in vivo CRISPR screens. *Science* **373**, 1146–1151.

672 **Pi, M. and Quarles, L. D.** (2012). GPRC6A regulates prostate cancer progression.
673 *Prostate* **72**, 399–409.

674 **Pi, M., Faber, P., Ekema, G., Jackson, P. D., Ting, A., Wang, N., Fontilla-Poole, M.,**
675 **Mays, R. W., Brunden, K. R., Harrington, J. J., et al.** (2005). Identification of a novel
676 extracellular cation-sensing G-protein-coupled receptor. *J. Biol. Chem.* **280**, 40201–
677 40209.

678 **Pi, M., Chen, L., Huang, M.-Z., Zhu, W., Ringhofer, B., Luo, J., Christenson, L., Li,**
679 **B., Zhang, J., Jackson, P. D., et al.** (2008). GPRC6A null mice exhibit osteopenia,
680 feminization and metabolic syndrome. *PLoS ONE* **3**, e3858.

681 **Pi, M., Parrill, A. L. and Quarles, L. D.** (2010). GPRC6A mediates the non-genomic
682 effects of steroids. *J. Biol. Chem.* **285**, 39953–39964.

683 **Pi, M., Kapoor, K., Wu, Y., Ye, R., Senogles, S. E., Nishimoto, S. K., Hwang, D.-J.,**
684 **Miller, D. D., Narayanan, R., Smith, J. C., et al.** (2015). Structural and functional
685 evidence for testosterone activation of GPRC6A in peripheral tissues. *Mol.*
686 *Endocrinol.* **29**, 1759–1773.

687 **Pi, M., Kapoor, K., Ye, R., Smith, J. C., Baudry, J. and Quarles, L. D.** (2018).
688 GPCR6A is a molecular target for the natural products gallate and EGCG in green
689 tea. *Mol. Nutr. Food Res.* **62**, e1700770.

690 **Romano, S. N., Edwards, H. E., Souder, J. P., Ryan, K. J., Cui, X. and Gorelick, D.**
691 **A.** (2017). G protein-coupled estrogen receptor regulates embryonic heart rate in
692 zebrafish. *PLoS Genet.* **13**, e1007069.

693 **Rosati, B., Yan, Q., Lee, M. S., Liou, S.-R., Ingalls, B., Foell, J., Kamp, T. J. and**
694 **McKinnon, D.** (2011). Robust L-type calcium current expression following
695 heterozygous knockout of the Cav1.2 gene in adult mouse heart. *J Physiol (Lond)*
696 **589**, 3275–3288.

697 **Rossetti, M. L., Steiner, J. L. and Gordon, B. S.** (2017). Androgen-mediated
698 regulation of skeletal muscle protein balance. *Mol. Cell. Endocrinol.* **447**, 35–44.

699 **Rottbauer, W., Baker, K., Wo, Z. G., Mohideen, M. A., Cantiello, H. F. and Fishman,**
700 **M. C.** (2001). Growth and function of the embryonic heart depend upon the cardiac-
701 specific L-type calcium channel alpha1 subunit. *Dev. Cell* **1**, 265–275.

702 **Scragg, J. L., Jones, R. D., Channer, K. S., Jones, T. H. and Peers, C.** (2004).
703 Testosterone is a potent inhibitor of L-type Ca(2+) channels. *Biochem. Biophys. Res.*
704 *Commun.* **318**, 503–506.

705 **Scragg, J. L., Dallas, M. L. and Peers, C.** (2007). Molecular requirements for L-type
706 Ca2+ channel blockade by testosterone. *Cell Calcium* **42**, 11–15.

707 **Seisenberger, C., Specht, V., Welling, A., Platzer, J., Pfeifer, A., Kühbandner, S.,**
708 **Striessnig, J., Klugbauer, N., Feil, R. and Hofmann, F.** (2000). Functional
709 embryonic cardiomyocytes after disruption of the L-type alpha1C (Cav1.2) calcium
710 channel gene in the mouse. *J. Biol. Chem.* **275**, 39193–39199.

711 **Serobyan, V., Kontarakis, Z., El-Brolosy, M. A., Welker, J. M., Tolstenkov, O.,**
712 **Saadeldein, A. M., Retzer, N., Gottschalk, A., Wehman, A. M. and Stainier, D. Y.**
713 (2020). Transcriptional adaptation in Caenorhabditis elegans. *eLife* **9**,.

714 **Shivaji, S. and Jagannadham, M. V.** (1992). Steroid-induced perturbations of
715 membranes and its relevance to sperm acrosome reaction. *Biochim. Biophys. Acta*
716 **1108**, 99–109.

717 **Sula, A., Hollingworth, D., Ng, L. C. T., Larmore, M., DeCaen, P. G. and Wallace, B.**
718 **A.** (2021). A tamoxifen receptor within a voltage-gated sodium channel. *Mol. Cell*.

719 **Sun, Y.-H., Gao, X., Tang, Y.-J., Xu, C.-L. and Wang, L.-H.** (2006). Androgens induce
720 increases in intracellular calcium via a G protein-coupled receptor in LNCaP prostate
721 cancer cells. *J. Androl.* **27**, 671–678.

722 **Thomas, P.** (2019). Membrane androgen receptors unrelated to nuclear steroid
723 receptors. *Endocrinology* **160**, 772–781.

724 **Thomas, P., Pang, Y., Dong, J. and Berg, A. H.** (2014). Identification and
725 characterization of membrane androgen receptors in the ZIP9 zinc transporter
726 subfamily: II. Role of human ZIP9 in testosterone-induced prostate and breast cancer
727 cell apoptosis. *Endocrinology* **155**, 4250–4265.

728 **Tilley, W. D., Marcelli, M., Wilson, J. D. and McPhaul, M. J.** (1989). Characterization
729 and expression of a cDNA encoding the human androgen receptor. *Proc Natl Acad*
730 *Sci U S A* **86**, 327–31.

731 **Trapman, J., Klaassen, P., Kuiper, G. G., van der Korput, J. A., Faber, P. W., van**
732 **Rooij, H. C., Geurts van Kessel, A., Voorhorst, M. M., Mulder, E. and Brinkmann,**
733 **A. O.** (1988). Cloning, structure and expression of a cDNA encoding the human
734 androgen receptor. *Biochem. Biophys. Res. Commun.* **153**, 241–248.

735 **Treviño, L. S. and Gorelick, D. A.** (2021). The interface of nuclear and membrane
736 steroid signaling. *Endocrinology* **162**,.

**Westerfield, M.** (2000). *The Zebrafish Book. A Guide for the Laboratory Use of Zebrafish (Danio Rerio).* 4th ed. Eugene, OR: University of Oregon Press.

**Whiting, K. P., Brain, P. F. and Restall, C. J.** (1995). Steroid hormone induced effects on membrane fluidity. *Biochem. Soc. Trans.* **23**, 438S.

**Whiting, K. P., Restall, C. J. and Brain, P. F.** (2000). Steroid hormone-induced effects on membrane fluidity and their potential roles in non-genomic mechanisms. *Life Sci.* **67**, 743–757.

**Wunderlich, F., Benten, W. P. M., Lieberherr, M., Guo, Z., Stamm, O., Wrehlke, C., Sekeris, C. E. and Mossmann, H.** (2002). Testosterone signaling in T cells and macrophages. *Steroids* **67**, 535–538.

**Wu, R. S., Lam, I. I., Clay, H., Duong, D. N., Deo, R. C. and Coughlin, S. R.** (2018). A rapid method for directed gene knockout for screening in G0 zebrafish. *Dev. Cell* **46**, 112-125.e4. Sciwheel inserting bibliography...

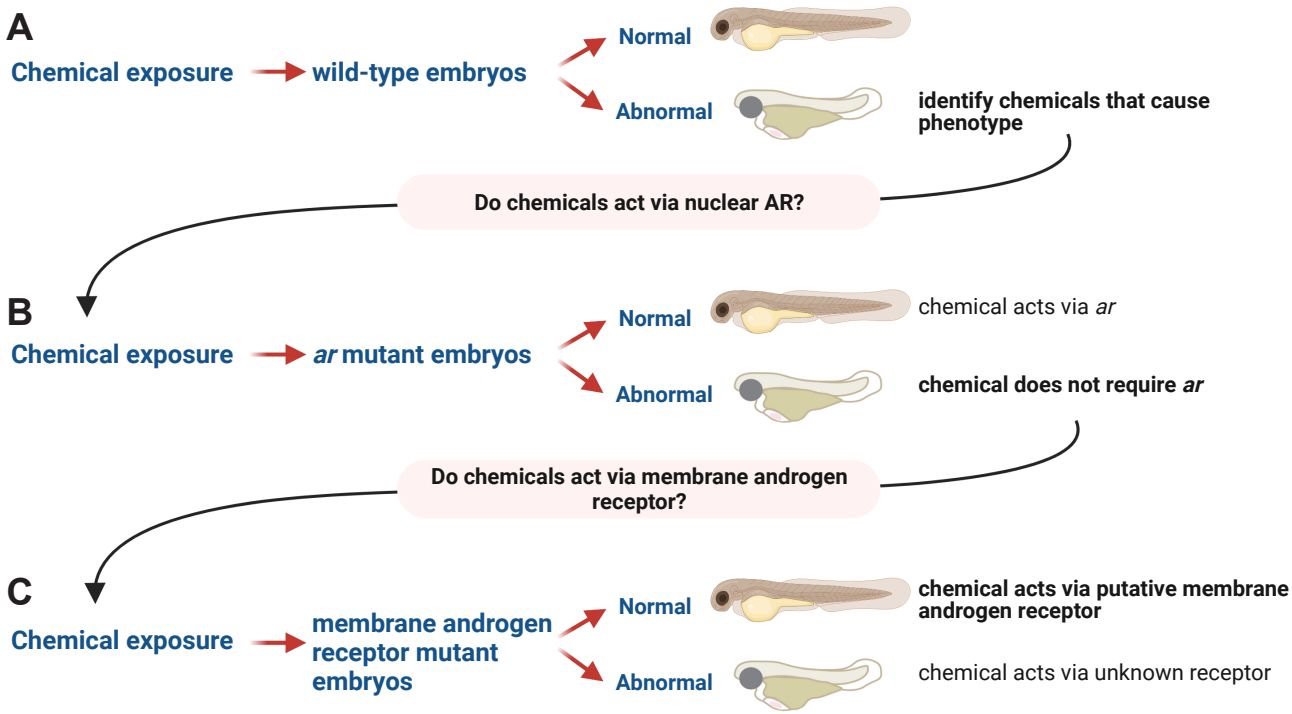


**Figure 1. Chemical-genetic screen to identify receptors that mediate androgen-dependent phenotypes.** **(A)** We exposed wild-type embryos to multiple androgens at different concentrations beginning at 3 hours post fertilization. We assayed embryo morphology at 2- and 3- days post fertilization. We identified chemicals that caused morphologic abnormalities. **(B)** We tested whether the phenotype is rescued in zebrafish with mutations in the nuclear androgen receptor gene (*ar*). If the phenotype is rescued, then the steroid acts via AR. **(C)** If the phenotype persists in the nuclear *ar* mutant, then we test zebrafish with mutations in membrane steroid receptors. To efficiently generate membrane androgen receptor mutants, we inject embryos with Cas9 and guide RNAs, expose injected embryos to chemicals, and screen for phenotypes. Following phenotypic screening, embryos are genotyped to determine mutation burden. Figure created using BioRender.com.

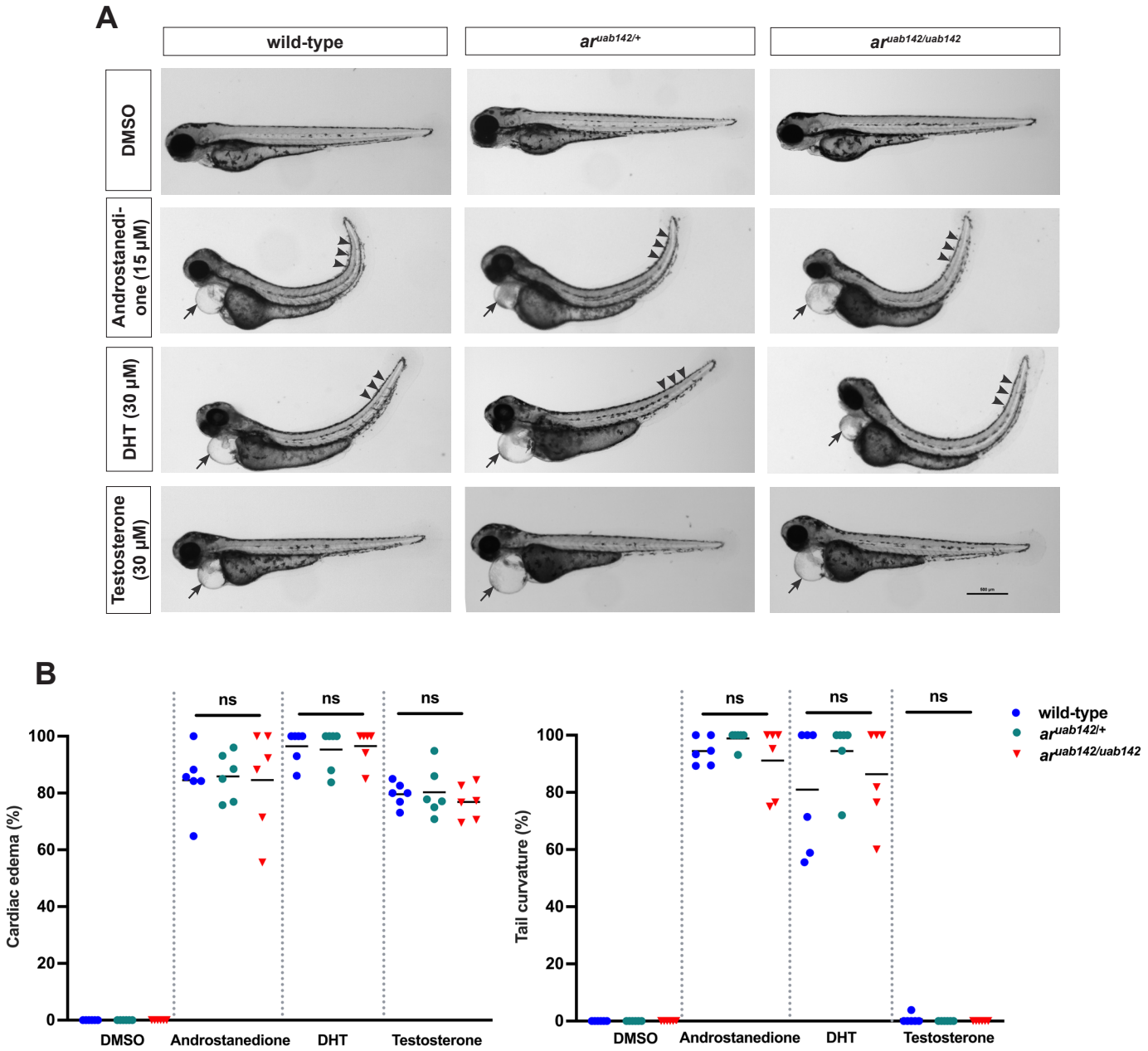


**Figure 2. Identification of androgens that cause phenotypes in wild-type and nuclear androgen receptor (*ar*) mutant embryos.** Wild-type or ar mutant embryos were exposed to vehicle (0.1% DMSO), 5α-Androstane-3,17-dione (androstanedione), dihydrotestosterone (DHT), or testosterone beginning at 3 hours post fertilization. (A) Representative images of embryos at 3 days post fertilization. Note cardiac edema (arrows) and tail curvature (arrowheads). Each clutch was derived from heterozygous parents and contained a mix of wild-type, heterozygous ar uab142/+, or homozygous ar uab142/uab142 embryos. Lateral views with anterior to the left, dorsal to the top. Scale bar = 500 µm. (B) Percent of embryos exhibiting cardiac edema or tail curvature. Each data point is the mean percent of embryos in a single clutch exhibiting cardiac edema or tail curvature (11-57 embryos per clutch). Clutches in the same treatment group were assayed on different days. Genotypes and treatments are separated by vertical gray dotted lines in each graph. Horizontal lines are the mean of each treatment. ns, not significant ($p > .05$), one-way ANOVA with Tukey's multiple comparisons test.

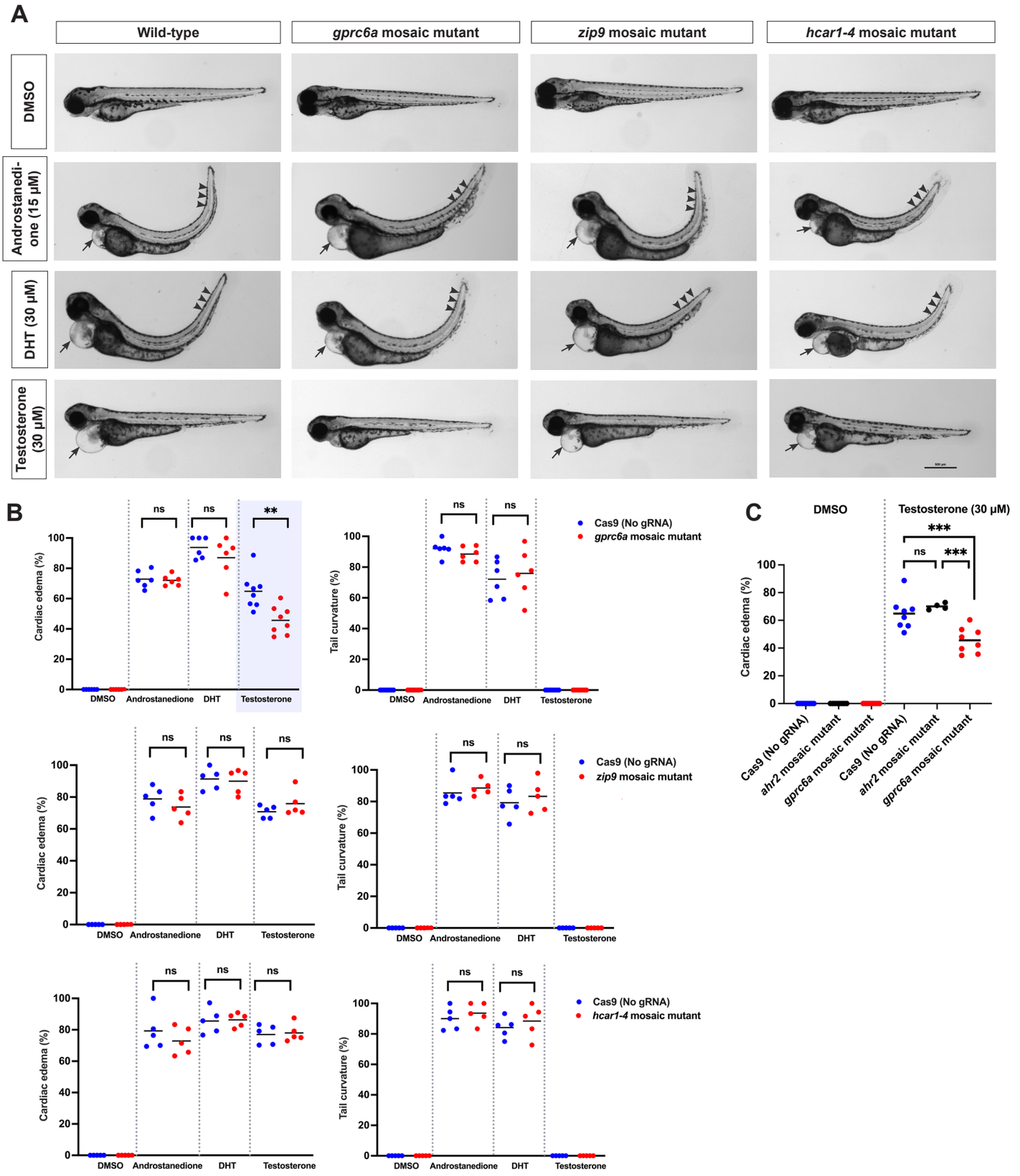


**Figure 3. Testosterone phenotype is partially rescued by CRISPR targeting *gprc6a*.** 1-cell stage embryos were injected with Cas9 protein alone or together with a cocktail of 4 guide RNAs targeting different regions of the indicated genes (*gprc6a*, *zip9*, *hcar1-4*). At 3 hours post fertilization, embryos were exposed to vehicle (0.1% DMSO), 5α-Androstane-3,17-dione (androstanedione), dihydrotestosterone (DHT), or testosterone. **(A)** Representative images of embryos at 3 days post fertilization. Note cardiac edema (arrows) and curved tail (arrowheads), except in *gprc6a* mosaic mutants following testosterone exposure. Lateral views with anterior to the left, dorsal to the top. Scale bars = 500 µm. **(B)** Percent of embryos exhibiting cardiac edema (left graphs) or tail curvature (right graphs). Each data point is the percent of embryos in a single clutch exhibiting cardiac edema or tail curvature (25-160 embryos per clutch). Clutches in the same treatment group were assayed on different days. Genotypes and treatments are separated by vertical gray dotted lines in each graph. Horizontal lines are the mean of each treatment. **(C)** As an additional control, embryos were injected with Cas9 protein alone or with guide RNAs targeting an unrelated gene *(ahr2),* and then exposed to vehicle or testosterone. The percent of embryos with cardiac edema was assayed at 3 days post fertilization. Each data point represents a single clutch (35-70 embryos per clutch). ns, not significant ($p > .05$), $^{**}p < .01$, $^{***}p < .001$, one-way ANOVA with Tukey's multiple comparisons test.

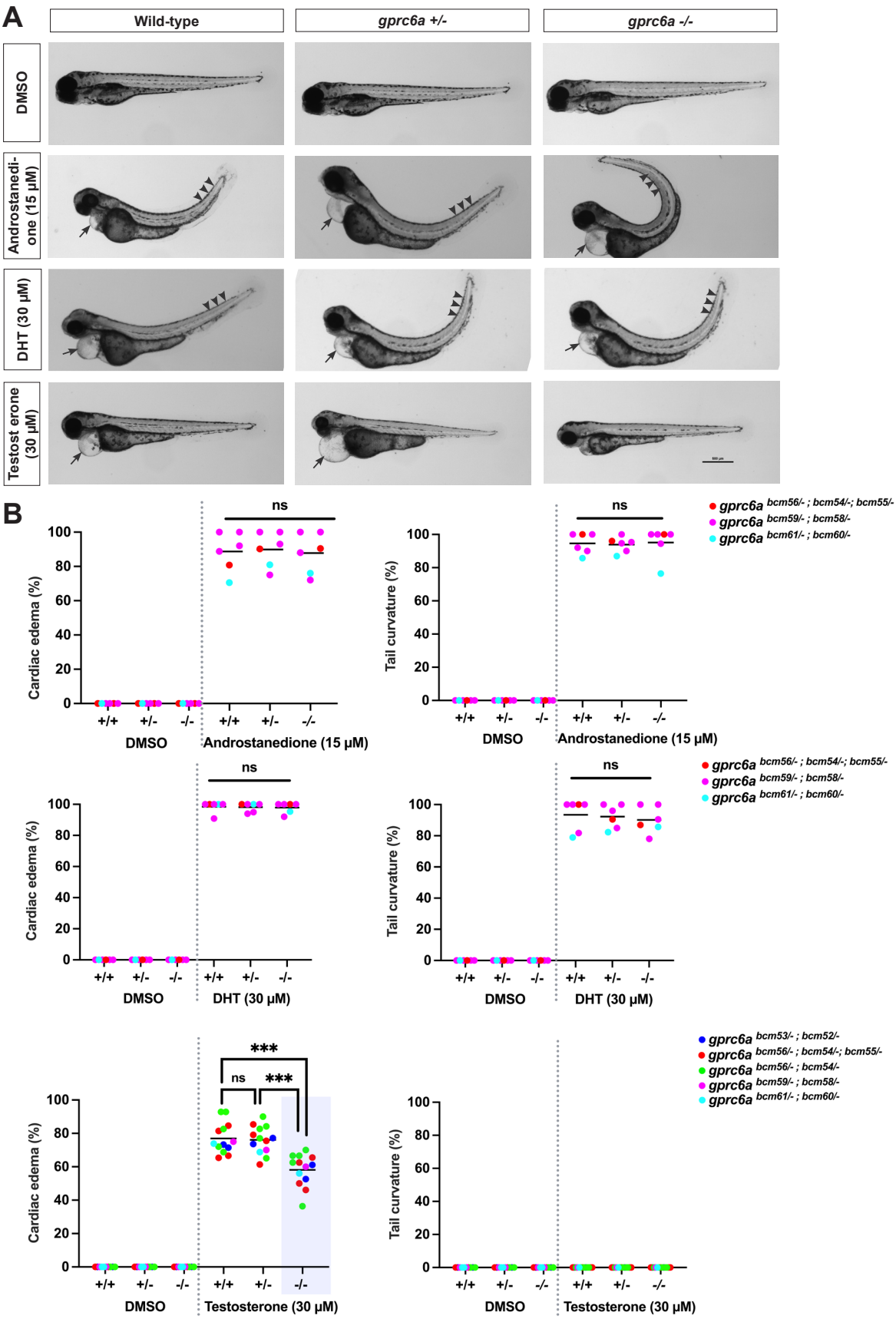


**Figure 4. Testosterone phenotype is partially rescued in homozygous *gprc6a* mutants**. Heterozygous *gprc6a* adult zebrafish were crossed to each other to generate zygotic *gprc6a* mutants. The clutch contained a mix of wild-type and mutant embryos (denoted as wild-type +/+, heterozygous +/-, or homozygous -/-). Embryos were exposed to vehicle (0.1% DMSO) or 5α-Androstane-3,17-dione (androstanedione), dihydrotestosterone (DHT), and testosterone beginning at 3 hours post fertilization. Morphologic phenotypes were assayed at 3 days post fertilization, then each embryo was genotyped. **(A)** Representative images of *gprc6a* $^{bcm56/-; bcm54/-; bcm55/-}$ embryos at 3 days post fertilization. Note cardiac edema (arrows) and curved tail (arrowheads), except in homozygous *gprc6a* mutants following testosterone exposure. Lateral views with anterior to the left, dorsal to the top. Scale bars = 500 µm. **(B)** Percent of embryos exhibiting cardiac edema (left graph) or tail curvature (right graph). Each data point is the mean percent of embryos in a single clutch exhibiting cardiac edema or tail curvature (15-50 embryos per clutch). Clutches in the same treatment group were assayed on different days. Horizontal lines are the mean of each group. Five independently generated zygotic mutant lines are shown, where each line is a different color and each allele designation indicates a unique DNA mutation. ***$p < .001$, ns, not significant ($p > .05$), one-way ANOVA with Tukey's multiple comparisons test.

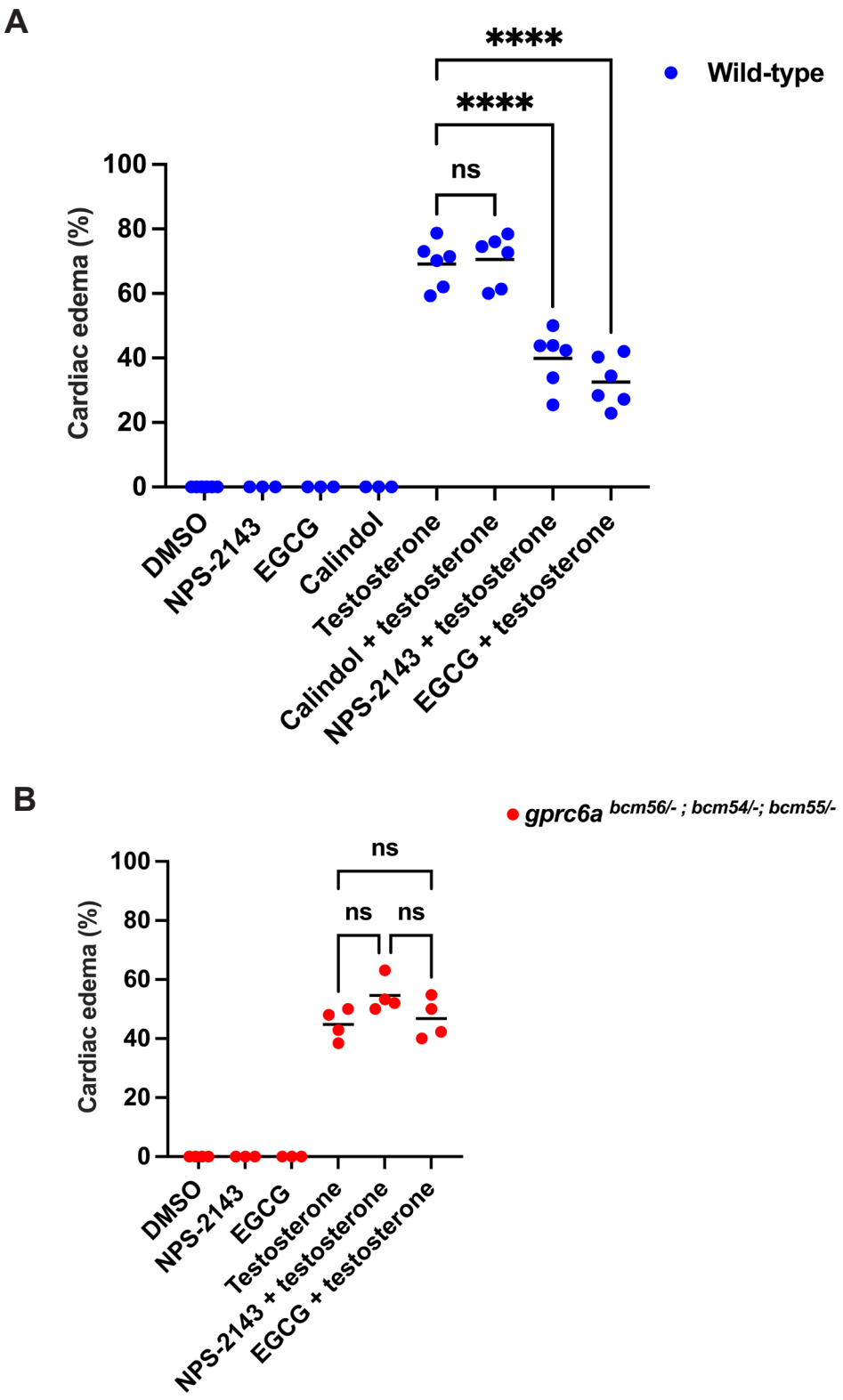


**Figure 5. GPRC6A antagonists rescue testosterone phenotype in wild-type embryos but have no effect in *gprc6a* mutants. (A)** Wild-type embryos were exposed to vehicle (0.1% DMSO) or GPRC6A antagonists: calindol (5 μM), NPS-2143 (5 μM), and epigallocatechin gallate (EGCG, 100 μM) with or without testosterone (30 μM) beginning at 3 hours post fertilization. Morphologic phenotypes were assayed at 3 days post fertilization. NPS-2143 and EGCG reduced cardiac edema following testosterone exposure. **(B)** Homozygous zygotic *gprc6a* mutant embryos were exposed to vehicle, NPS-2143 (5 μM), or EGCG (100 μM) with or without testosterone (30 μM) beginning at 3 hours post fertilization. Morphologic phenotypes were assayed at 3 days post fertilization. Antagonists failed to reduce cardiac edema in *gprc6a* mutant embryos. Each data point is the mean percent of embryos in a single clutch exhibiting cardiac edema (15-25 embryos per clutch). Clutches in the same treatment group were assayed on different days. Horizontal lines are the mean of each group. ****$p < .0001$, ns, not significant ($p > .05$), one-way ANOVA with Tukey's multiple comparisons test.

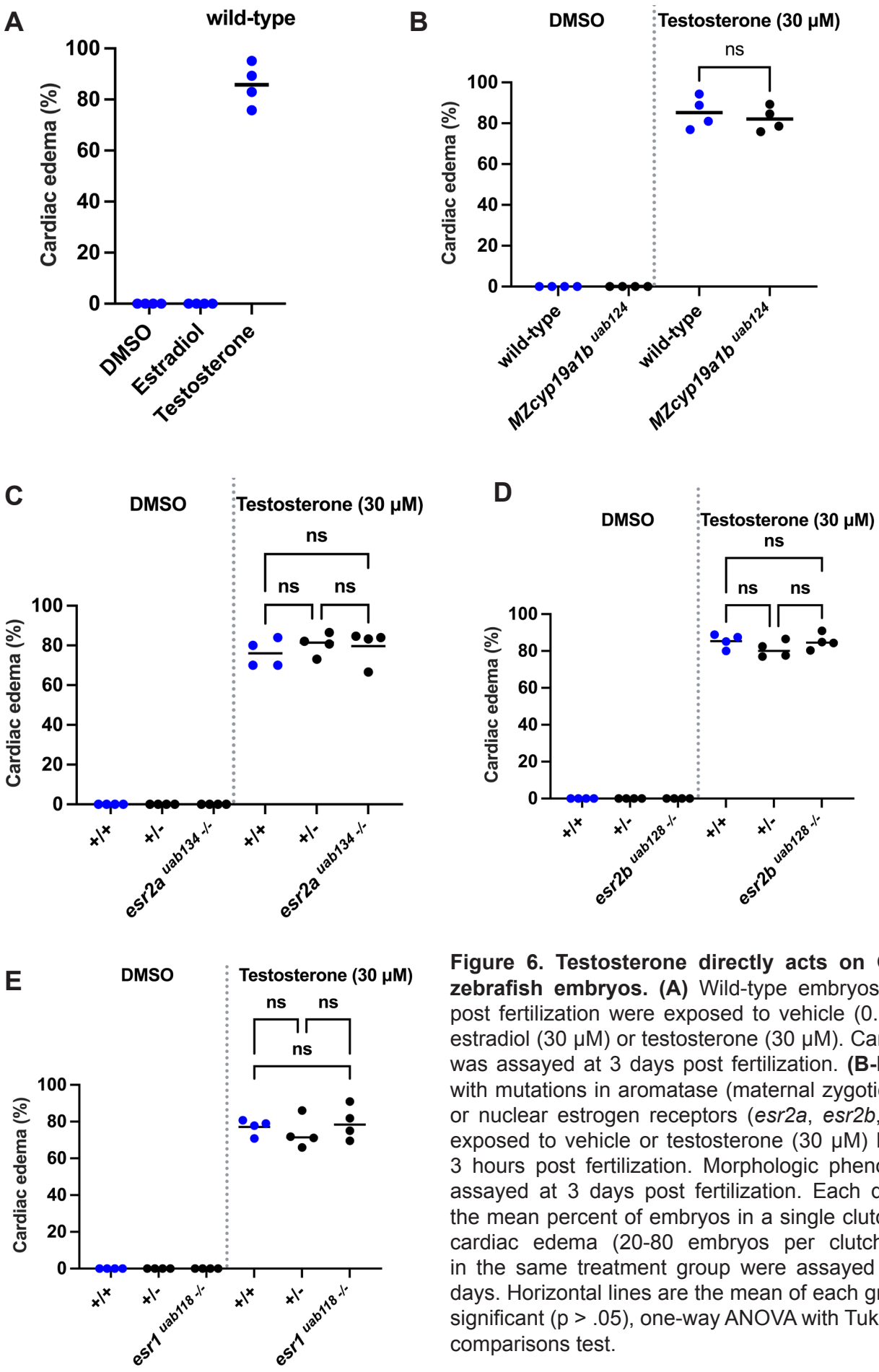


**Figure 6. Testosterone directly acts on GPRC6A in zebrafish embryos. (A)** Wild-type embryos at 3 hours post fertilization were exposed to vehicle (0.1% DMSO), estradiol (30 μM) or testosterone (30 μM). Cardiac edema was assayed at 3 days post fertilization. **(B-E)** Zebrafish with mutations in aromatase (maternal zygotic *cyp19a1b*) or nuclear estrogen receptors (*esr2a*, *esr2b*, *esr1*) were exposed to vehicle or testosterone (30 μM) beginning at 3 hours post fertilization. Morphologic phenotypes were assayed at 3 days post fertilization. Each data point is the mean percent of embryos in a single clutch exhibiting cardiac edema (20-80 embryos per clutch). Clutches in the same treatment group were assayed on different days. Horizontal lines are the mean of each group. ns, not significant ($p > .05$), one-way ANOVA with Tukey's multiple comparisons test.

| Genotype | Clutch (biological replicate) | Treatment | Number of embryos/clutch | % Cardiac edema, 3 dpf | Mean % embryos with cardiac edema | Standard deviation (cardiac edema) | % Tail curvature, 3 dpf | Mean % embryos with tail curvature | Standard deviation (tail curvature) | % Cardiac edema + tail curvature, 3 dpf | % Normal embryos, 3 dpf | Notes |
|---|---|---|---|---|---|---|---|---|---|---|---|---|
| Wild-type | n = 6 | 0.1% DMSO | 12,10,12,14,10,10 | 0,0,0,0,0,0 | 0 | 0 | 0,0,0,0,0,0 | 0 | 0 | 0,0,0,0,0,0 | 100,100,100,100,100,000 | Pictured in Fig. 2 |
| Heterozygous *ar* $^{uab142/+}$ | n = 6 | 0.1% DMSO | 25,24,22,26,23,25 | 0,0,0,0,0,0 | 0 | 0 | 0,0,0,0,0,0 | 0 | 0 | 0,0,0,0,0,0 | 100,100,100,100,100,000 | Pictured in Fig. 2 |
| homozygous *ar* $^{uab142/uab142}$ | n = 6 | 0.1% DMSO | 10,12,11,10,14,10 | 0,0,0,0,0,0 | 0 | 0 | 0,0,0,0,0,0 | 0 | 0 | 0,0,0,0,0,0 | 100,100,100,100,100,000 | Pictured in Fig. 2 |
| Wild-type | n = 6 | 15 μM androstanedione | 15,19,15,19,17,12 | 64,84,85,84,88,100 | 84 | 12 | 94,89,89,100,100,93 | 94 | 5 | 64,84,85,84,88,100 | 6,11,11,0,0,0 | Pictured in Fig. 2 |
| Heterozygous *ar* $^{uab142/+}$ | n = 6 | 15 μM androstanedione | 33,26,29,39,25,20 | 75,88,93,76,96,85 | 86 | 9 | 100,100,93,100,100,100 | 99 | 3 | 75,88,93,76,96,85 | 0,0,7,0,0,0 | Pictured in Fig. 2 |
| homozygous *ar* $^{uab142/uab142}$ | n = 6 | 15 μM androstanedione | 17,12,13,21,17,13 | 88,100,55,71,100,92 | 84 | 16 | 76,75,100,95,100,100 | 91 | 11 | 88,100,55,71,100,92 | 12,0,0,5,0,0 | Pictured in Fig. 2 |
| Wild-type | n = 6 | 30 μM DHT | 20,27,25,18,20,13 | 86,92,100,100,100,100 | 96 | 5 | 55,58,71,100,100,100 | 81 | 20 | 86,92,100,100,100,100 | 14,8,0,0,0,0 | Pictured in Fig. 2 |
| Heterozygous *ar* $^{uab142/+}$ | n = 6 | 30 μM DHT | 37,57,50,48,48,25 | 83,100,88,100,100,100 | 95 | 7 | 94,100,72,100,100,100 | 94 | 10 | 83,100,88,100,100,100 | 6,0,12,0,0,0 | Pictured in Fig. 2 |
| homozygous *ar* $^{uab142/uab142}$ | n = 6 | 30 μM DHT | 20,25,15,20,22,13 | 85,100,94,100,100,100 | 97 | 6 | 60,81,76,100,100,100 | 86 | 15 | 85,100,94,100,100,100 | 15,0,6,0,0,0 | Pictured in Fig. 2 |
| Wild-type | n = 6 | 30 μM Testosterone | 15,23,26,20,26,20 | 80,82,76,85,73,80 | 79 | 4 | 0,0,0,0,0,0 | 0 | 0 | 0,0,0,0,0,0 | 20,17,23,15,26,20 | Pictured in Fig. 2 |
| Heterozygous *ar* $^{uab142/+}$ | n = 6 | 30 μM Testosterone | 50,36,39,48,40,48 | 86,77,94,70,75,77 | 80 | 8 | 0,0,0,0,0,0 | 0 | 0 | 0,0,0,0,0,0 | 14,22,5,29,25,22 | Pictured in Fig. 2 |
| homozygous *ar* $^{uab142/uab142}$ | n = 6 | 30 μM Testosterone | 13,17,23,23,30,22 | 84,70,69,82,76,77 | 76 | 6 | 0,0,0,0,0,0 | 0 | 0 | 0,0,0,0,0,0 | 15,29,30,17,23,22 | Pictured in Fig. 2 |

**Table 1.** Embryo data accompanying Figure 2.

| Genotype | Clutch (biological replicate) | Treatment | Number of embryos/clutch | % Cardiac edema, 3 dpf | Mean % embryos with cardiac edema | Standard deviation (cardiac edema) | % Tail curvature, 3 dpf | Mean % embryos with tail curvature | Standard deviation (tail curvature) | % Cardiac edema + tail curvature, 3 dpf | % Normal embryos, 3 dpf | Notes |
|---|---|---|---|---|---|---|---|---|---|---|---|---|
| wild-type | n = 6 | 0.1% DMSO | 22,24,10,22,22,24 | 0,0,0,0,0,0 | 0 | 0 | 0,0,0,0,0,0 | 0 | 0 | 0,0,0,0,0,0 | 100,100,100,100,100,100, | Pictured in Fig. 3 |
| *gprc6a* mosaic mutant | n = 6 | 0.1% DMSO | 10,10,22,14,24,22 | 0,0,0,0,0,0 | 0 | 0 | 0,0,0,0,0,0 | 0 | 0 | 0,0,0,0,0,0 | 100,100,100,100,100,100, | Pictured in Fig. 3 |
| *ahr2* mosaic mutant | n = 4 | 0.1% DMSO | 24,12,22,16 | 0,0,0,0 | 0 | 0 | 0,0,0,0 | 0 | 0 | 0,0,0,0 | 100,100,100,100, | Pictured in Fig. 3 |
| Wild-type | n = 5 | 0.1% DMSO | 14,20,10,22,20 | 0,0,0,0,0 | 0 | 0 | 0,0,0,0,0 | 0 | 0 | 0,0,0,0,0 | 100,100,100,100,100, | Pictured in Fig. 3 |
| *zip9* mosaic mutant | n = 5 | 0.1% DMSO | 11,10,22,14,14 | 0,0,0,0,0 | 0 | 0 | 0,0,0,0,0 | 0 | 0 | 0,0,0,0,0 | 100,100,100,100,100, | Pictured in Fig. 3 |
| Wild-type | n = 5 | 0.1% DMSO | 12,10,10,22,20 | 0,0,0,0,0 | 0 | 0 | 0,0,0,0,0 | 0 | 0 | 0,0,0,0,0 | 100,100,100,100,100, | Pictured in Fig. 3 |
| *hcar1-4* mosaic mutant | n = 5 | 0.1% DMSO | 23,22,20,20,14 | 0,0,0,0,0 | 0 | 0 | 0,0,0,0,0 | 0 | 0 | 0,0,0,0,0 | 100,100,100,100,100, | Pictured in Fig. 3 |
| wild-type | n = 6 | 15 µM androstanedione | 115,32,50,36,36,26 | 78,68,72,80,72,65 | 73 | 6 | 93,100,92,91,83,92 | 92 | 5 | 78,68,72,80,72,65 | 7,0,8,9,17,8 | Pictured in Fig. 3 |
| *gprc6a* mosaic mutant | n = 6 | 15 µM androstanedione | 38,34,34,36,36,38 | 68,73,68,77,72,71 | 72 | 3 | 86,94,93,83,83,89 | 88 | 5 | 68,73,68,77,72,71 | 14,6,7,17,17,11 | Pictured in Fig. 3 |
| Wild-type | n = 5 | 15 µM androstanedione | 36,30,33,30,33 | 80,66,87,83,75 | 78 | 8 | 100,83,78,83,81 | 85 | 9 | 80,66,87,83,75 | 0,17,13,17,19 | Pictured in Fig. 3 |
| *zip9* mosaic mutant | n = 5 | 15 µM androstanedione | 48,36,40,40,36 | 79,83,70,72,63 | 73 | 8 | 95,86,90,87,83 | 88 | 5 | 79,83,70,72,63 | 5,14,10,13,17 | Pictured in Fig. 3 |
| Wild-type | n = 5 | 15 µM androstanedione | 36,30,30,34,36 | 80,100,70,76,69 | 79 | 13 | 83,90,100,82,94 | 90 | 8 | 80,100,70,76,69 | 17,0,0,18,6 | Pictured in Fig. 3 |
| *hcar1-4* mosaic mutant | n = 5 | 15 µM androstanedione | 3,30,35,36,35 | 63,83,65,80,71 | 72 | 9 | 100,93,100,83,91 | 93 | 7 | 63,83,65,80,71 | 0,7,0,7,9 | Pictured in Fig. 3 |
| wild-type | n = 6 | 30 µM DHT | 93,46,48,36,30,36 | 90,86,85,100,100,100 | 94 | 7 | 59,67,58,83,86,77 | 72 | 12 | 90,86,85,100,100,100 | 10,14,15,0,0,0 | Pictured in Fig. 3 |
| *gprc6a* mosaic mutant | n = 6 | 30 µM DHT | 27,40,36,40,36,31 | 62,90,80,95,100,93 | 87 | 14 | 51,87,66,75,77,96 | 75 | 16 | 62,90,80,95,100,93 | 38,10,20,5,0,4 | Pictured in Fig. 3 |
| Wild-type | n = 5 | 30 µM DHT | 40,30,35,30,35 | 100,93,94,83,85 | 91 | 7 | 90,86,77,76,65 | 79 | 10 | 100,93,94,83,85 | 0,7,6,17,15 | Pictured in Fig. 3 |
| *zip9* mosaic mutant | n = 5 | 30 µM DHT | 25,30,40,40,36 | 80,96,95,95,83 | 90 | 8 | 97,83,72,87,75 | 83 | 10 | 80,96,95,95,83 | 3,4,5,5,17 | Pictured in Fig. 3 |
| Wild-type | n = 5 | 30 µM DHT | 36,29,35,36,30 | 88,79,85,97,76 | 85 | 8 | 75,86,85,80,93 | 84 | 7 | 88,79,85,97,76 | 12,14,15,3,7 | Pictured in Fig. 3 |
| *hcar1-4* mosaic mutant | n = 5 | 30 µM DHT | 33,36,35,36,35 | 90,88,82,80,88 | 86 | 4 | 72,91,94,83,100 | 88 | 11 | 90,88,82,80,88 | 10,9,6,17,0 | Pictured in Fig. 3 |
| wild-type | n = 8 | 30 µM Testosterone | 90,75,82,53,59,42,53,50 | 51,56,62,56,69,66,88,68 | 65 | 11 | 0,0,0,0,0,0,0,0 | 0 | 0 | 0,0,0,0,0,0,0,0 | 49,44,38,44,31,34,12,32 | Pictured in Fig. 3 |
| *gprc6a* mosaic mutant | n = 8 | 30 µM Testosterone | 164,87,90,81,73,96,72,88 | 34,35,42,39,47,60,51,53 | 45 | 9 | 0,0,0,0,0,0,0,0 | 0 | 0 | 0,0,0,0,0,0,0,0 | 65,65,58,52,50,40,49,47 | Pictured in Fig. 3 |
| *ahr2* mosaic mutant | n = 4 | 30 µM Testosterone | 48,72,34,48 | 72,70,67,68 | 69 | 2 | 0,0,0,0,0 | 0 | 0 | 0,0,0,0,0 | 28,30,33,32 | Pictured in Fig. 3 |
| Wild-type | n = 5 | 30 µM Testosterone | 34,60,50,68,60 | 73,66,72,75,66 | 70 | 4 | 0,0,0,0,0 | 0 | 0 | 0,0,0,0,0 | 27,34,28,25,34 | Pictured in Fig. 3 |
| *zip9* mosaic mutant | n = 5 | 30 µM Testosterone | 60,95,96,95,48 | 70,70,71,76,89 | 75 | 8 | 0,0,0,0,0 | 0 | 0 | 0,0,0,0,0 | 30,30,29,24,11 | Pictured in Fig. 3 |
| Wild-type | n = 5 | 30 µM Testosterone | 58,47,48,48,49 | 70,70,83,79,81 | 77 | 6 | 0,0,0,0,0 | 0 | 0 | 0,0,0,0,0 | 30,30,17,21,19 | Pictured in Fig. 3 |
| hcar1-4 mosaic mutant | n = 5 | 30 µM Testosterone | 96,82,48,48,48 | 72,75,87,75,79 | 78 | 6 | 0,0,0,0,0 | 0 | 0 | 0,0,0,0,0 | 28,25,13,25,21 | Pictured in Fig. 3 |

**Table 2.** Embryo data accompanying Figure 3. Wild-type embryos were injected with Cas9 protein without any gRNAs

| Genotype | Clutch (biological replicate) | Treatment | Number of embryos/clutch | % Cardiac edema, 3 dpf | Mean % embryos with cardiac edema | Standard deviation (cardiac edema) | % Tail curvature, 3 dpf | Mean % embryos with tail curvature | Standard deviation (tail curvature) | % Cardiac edema + tail curvature, 3 dpf | % Normal embryos, 3 dpf | Notes |
|---|---|---|---|---|---|---|---|---|---|---|---|---|
| Wild-type | n = 10 | 0.1% DMSO | 12,16,10,14,20,22,10,12,10,12 | 0,0,0,0,0,0,0,0,0,0 | 0 | 0 | 0,0,0,0,0,0,0,0,0,0 | 0 | 0 | 0,0,0,0,0,0,0,0,0,0 | 100,100,100,100,100,100,100,100,100,100, | Pictured in Fig. 4 |
| heterozygous *gprc6a* | n = 10 | 0.1% DMSO | 20,30,20,31,42,42,20,22,24,22 | 0,0,0,0,0,0,0,0,0,0 | 0 | 0 | 0,0,0,0,0,0,0,0,0,0 | 0 | 0 | 0,0,0,0,0,0,0,0,0,0 | 100,100,100,100,100,100,100,100,100,100, | Pictured in Fig. 4 |
| homozygous *gprc6a* | n = 10 | 0.1% DMSO | 14,16,10,18,20,20,10,12,11,12 | 0,0,0,0,0,0,0,0,0,0 | 0 | 0 | 0,0,0,0,0,0,0,0,0,0 | 0 | 0 | 0,0,0,0,0,0,0,0,0,0 | 100,100,100,100,100,100,100,100,100,100, | Pictured in Fig. 4 |
| Wild-type | n = 6 | 15 µM androstanedione | 20,21,20,26,18,25 | 88,70,80,100,100,92 | 88 | 12 | 90,85,100,100,100,92 | 95 | 6 | 88,70,80,100,100,92 | 10,15,0,0,0,8 | Pictured in Fig. 4 |
| heterozygous *gprc6a* | n = 6 | 15 µM androstanedione | 50,46,40,51,38,39 | 75,80,90,100,100,93 | 90 | 10 | 90,86,96,94,100,95 | 94 | 5 | 75,80,90,100,100,93 | 10,14,4,0,0,5 | Pictured in Fig. 4 |
| homozygous *gprc6a* | n = 6 | 15 µM androstanedione | 18,17,18,21,15,19 | 72,76,,90,100,100,88 | 88 | 12 | 94,76,100,100,100,100 | 95 | 10 | 72,76,,90,100,100,88 | 6,24,0,0,0,0 | Pictured in Fig. 4 |
| Wild-type | n = 6 | 30 µM DHT | 20,17,24,19,18,21 | 90,100,100,100,100,100 | 98 | 4 | 81,78,100,100,100,100 | 93 | 11 | 90,100,100,100,100,100 | 10,0,0,0,0,0 | Pictured in Fig. 4 |
| heterozygous *gprc6a* | n = 6 | 30 µM DHT | 50,42,54,42,42,36 | 95,100,100,100,100,94 | 98 | 3 | 85,82,90,100,100,96 | 92 | 8 | 95,100,100,100,100,94 | 5,0,0,0,0,4 | Pictured in Fig. 4 |
| homozygous *gprc6a* | n = 6 | 30 µM DHT | 22,19,21,23,25,22 | 92,95,100,100,100,100 | 98 | 3 | 78,85,86,100,100,90 | 90 | 9 | 92,95,100,100,100,100 | 8,5,0,0,0,0 | Pictured in Fig. 4 |
| Wild-type | n = 13 | 30 µM Testosterone | 15,26,25,12,28,16,27,23,21,26,14,20,23 | 73,71,65,66,81,84,72,92,68,82,92,75,73 | 76 | 9 | 0,0,0,0,0,0,0,0,0,0,0,0,0 | 0 | 0 | 0,0,0,0,0,0,0,0,0,0,0,0,0 | 27,29,35,34,19,16,28,8,32,18,8,27,27 | Pictured in Fig. 4 |
| heterozygous *gprc6a* | n = 13 | 30 µM Testosterone | 38,44,43,24,50,48,45,52,57,41,38,50,48 | 73,77,61,79,75,85,65,90,77,82,84,70,68 | 76 | 8 | 0,0,0,0,0,0,0,0,0,0,0,0,0 | 0 | 0 | 0,0,0,0,0,0,0,0,0,0,0,0,0 | 27,23,39,21,25,15,35,10,23,18,16,30,32 | Pictured in Fig. 4 |
| homozygous *gprc6a* | n = 13 | 30 µM Testosterone | 19,26,22,12,18,32,24,21,18,29,20,26,25 | 52,61,46,50,62,65,36,66,62,66,70,60,56 | 58 | 10 | 0,0,0,0,0,0,0,0,0,0,0,0,0 | 0 | 0 | 0,0,0,0,0,0,0,0,0,0,0,0,0 | 48,39,54,50,38,35,64,34,38,34,35,40,44 | Pictured in Fig. 4 |
| Wild-type | n = 13 | 30 µM Testosterone | 15,26,25,12,28,16,27,23,21,26,14,20,23 | 73,71,65,66,81,84,72,92,68,82,92,75,73 | 76 | 9 | 0,0,0,0,0,0,0,0,0,0,0,0,0 | 0 | 0 | 0,0,0,0,0,0,0,0,0,0,0,0,0 | 27,29,35,34,19,16,28,8,32,18,8,27,27 | Pictured in Fig. S4 |
| heterozygous *gprc6a* $^{bcm53/+;\ bcm52/+}$ | n = 2 | 30 µM Testosterone | 38,44 | 73,77 | 75 | 2 | 0,0 | 0 | 0 | 0,0 | 27,23 | Pictured in Fig. S4 |
| homozygous *gprc6a* $^{bcm53/-;\ bcm52/-}$ | n = 2 | 30 µM Testosterone | 19,26 | 52,61 | 57 | 5 | 0,0 | 0 | 0 | 0,0 | 48,39 | Pictured in Fig. S4 |
| heterozygous *gprc6a* $^{bcm56/+;\ bcm54/+;\ bcm55/+}$ | n = 4 | 30 µM Testosterone | 43,24,50,48 | 61,79,75,85 | 75 | 9 | 0,0,0,0 | 0 | 0 | 0,0,0,0 | 39,21,25,15 | Pictured in Fig. S4 |
| homozygous *gprc6a* $^{bcm56/-;\ bcm54/-;\ bcm55/-}$ | n = 4 | 30 µM Testosterone | 22,12,18,32 | 46,50,62,65 | 56 | 8 | 0,0,0,0 | 0 | 0 | 0,0,0,0 | 54,50,38,35 | Pictured in Fig. S4 |
| heterozygous *gprc6a* $^{bcm56/+;\ bcm54/+}$ | n = 5 | 30 µM Testosterone | 45,52,57,41,38 | 65,90,77,82,84 | 80 | 8 | 0,0,0,0,0 | 0 | 0 | 0,0,0,0,0 | 35,10,23,18,16 | Pictured in Fig. S4 |
| homozygous *gprc6a* $^{bcm56/-;\ bcm54/-}$ | n = 5 | 30 µM Testosterone | 24,21,18,29,20 | 36,66,62,66,70 | 60 | 12 | 0,0,0,0,0 | 0 | 0 | 0,0,0,0,0 | 64,34,38,34,35 | Pictured in Fig. S4 |
| heterozygous *gprc6a* $^{bcm59/+;\ bcm58/+}$ | n = 1 | 30 µM Testosterone | 50 | 70 | | | 0 | 0 | 0 | 0 | 30 | Pictured in Fig. S4 |
| homozygous *gprc6a* $^{bcm59/-;\ bcm58/-}$ | n = 1 | 30 µM Testosterone | 26 | 60 | | | 0 | 0 | 0 | 0 | 40 | Pictured in Fig. S4 |
| heterozygous *gprc6a* $^{bcm61/+;\ bcm60/+}$ | n = 1 | 30 µM Testosterone | 48 | 68 | | | 0 | 0 | 0 | 0 | 32 | Pictured in Fig. S4 |
| homozygous *gprc6a* $^{bcm61/-;\ bcm60/-}$ | n = 1 | 30 µM Testosterone | 25 | 56 | | | 0 | 0 | 0 | 0 | 44 | Pictured in Fig. S4 |

**Table 3.** Embryo data accompanying Figure 4 and Figure S4. The same data are pooled and grouped by gene (top table) or not pooled and grouped by allele (bottom table)

| Genotype | Clutch (biological replicate) | Treatment | Number of embryos/clutch | % Cardiac edema, 3 dpf | Mean % embryos with cardiac edema | Standard deviation (cardiac edema) | % Tail curvature, 3 dpf | % Cardiac edema + tail curvature, 3 dpf | % Normal embryos, 3 dpf | Notes |
|---|---|---|---|---|---|---|---|---|---|---|
| Wild-type | n = 6 | 0.1% DMSO | 30,40,28,32,25,25 | 0,0,0,0,0,0 | 0 | 0 | 0,0,0,0,0,0 | 0,0,0,0,0,0 | 100,100,100,100,100,100, | Pictured in Fig. 5 |
| Wild-type | n = 3 | 5 µM Calindol | 40,38,40 | 0,0,0 | 0 | 0 | 0,0,0 | 0,0,0 | 100,100,100 | Pictured in Fig. 5 |
| Wild-type | n = 3 | 5 µM NPS-2143 | 30,30,30 | 0,0,0 | 0 | 0 | 0,0,0 | 0,0,0 | 100,100,100 | Pictured in Fig. 5 |
| Wild-type | n = 3 | 100 µM EGCG | 40,40,40 | 0,0,0 | 0 | 0 | 0,0,0 | 0,0,0 | 100,100,100 | Pictured in Fig. 5 |
| Wild-type | n = 6 | 30 µM Testosterone | 50,59,63,47,52,57 | 62,59,71,78,73,70 | 69 | 7 | 0,0,0,0,0,0 | 0,0,0,0,0,0 | 38,41,29,22,27,37 | Pictured in Fig. 5 |
| Wild-type | n = 6 | 5 µM Calindol + 30 µM Testosterone | 50,55,59,51,57,44 | 76,60,74,78,61,72 | 70 | 8 | 0,0,0,0,0,0 | 0,0,0,0,0,0 | 24,40,26,22,39,28 | Pictured in Fig. 5 |
| Wild-type | n = 6 | 5 µM NPS-2143 + 30 µM Testosterone | 50,59,64,57,55,65 | 50,42,43,43,25,33 | 39 | 9 | 0,0,0,0,0,0 | 0,0,0,0,0,0 | 50,58,57,57,75,67 | Pictured in Fig. 5 |
| Wild-type | n = 6 | 100 µM EGCG + 30 µM Testosterone | 50,61,67,43,48,67 | 42,34,28,27,22,40 | 32 | 8 | 0,0,0,0,0,0 | 0,0,0,0,0,0 | 59,66,72,73,78,67 | Pictured in Fig. 5 |
| *gprc6a* $^{bcm56/-, bcm54/-, bcm55/-}$ | n = 4 | 0.1% DMSO | 26,20,34,22 | 0,0,0,0,0 | 0 | 0 | 0,0,0,0,0 | 0,0,0,0,0 | 100,100,100,100 | Pictured in Fig. 5 |
| *gprc6a* $^{bcm56/-, bcm54/-, bcm55/-}$ | n = 3 | 5 µM NPS-2143 | 20,30,30 | 0,0,0 | 0 | 0 | 0,0,0 | 0,0,0 | 100,100,100 | Pictured in Fig. 5 |
| *gprc6a* $^{bcm56/-, bcm54/-, bcm55/-}$ | n = 3 | 100 µM EGCG | 30,40,28 | 0,0,0 | 0 | 0 | 0,0,0 | 0,0,0 | 100,100,100 | Pictured in Fig. 5 |
| *gprc6a* $^{bcm56/-, bcm54/-, bcm55/-}$ | n = 4 | 30 µM Testosterone | 25,18,21,26 | 48,50,42,38 | 45 | 5 | 0,0,0,0 | 0,0,0,0 | 52,50,58,62 | Pictured in Fig. 5 |
| *gprc6a* $^{bcm56/-, bcm54/-, bcm55/-}$ | n = 4 | 5 µM NPS-2143 + 30 µM Testosterone | 25,24,30,19 | 52,50,53,63 | 55 | 5 | 0,0,0,0 | 0,0,0,0 | 48,50,47,37 | Pictured in Fig. 5 |
| *gprc6a* $^{bcm56/-, bcm54/-, bcm55/-}$ | n = 4 | 100 µM EGCG + 30 µM Testosterone | 26,22,24,24 | 42,40,50,54 | 47 | 6 | 0,0,0,0 | 0,0,0,0 | 58,60,50,46 | Pictured in Fig. 5 |

**Table 4.** Embryo data accompanying Figure 5.

| Genotype | Clutch (biological replicate) | Treatment | Number of embryos/clutch | % Cardiac edema, 3 dpf | Mean % embryos with cardiac edema | Standard deviation (cardiac edema) | % Tail curvature, 3 dpf | % Cardiac edema + tail curvature, 3 dpf | % Normal embryos, 3 dpf | Notes |
|---|---|---|---|---|---|---|---|---|---|---|
| Wild-type | n = 4 | 0.1% DMSO | 20,20,11,20 | 0,0,0,0 | 0 | 0 | 0,0,0,0 | 0,0,0,0 | 100,100,100,100 | Pictured in Fig. 6 |
| Wild-type | n = 4 | 30 µM Estradiol | 42,30,26,22 | 0,0,0,0 | 0 | 0 | 0,0,0,0 | 0,0,0,0 | 100,100,100,100 | Pictured in Fig. 6 |
| Wild-type | n = 4 | 30 µM Testosterone | 28,33,41,41 | 89,75,95,82 | 85 | 9 | 0,0,0,0 | 0,0,0,0 | 11,25,5,18 | Pictured in Fig. 6 |
| Wild-type | n = 4 | 0.1% DMSO | 20,25,24,19 | 0,0,0,0 | 0 | 0 | 0,0,0,0 | 0,0,0,0 | 100,100,100,100 | Pictured in Fig. 6 |
| *MZcyp19a1b* $^{uab124}$ | n = 4 | 0.1% DMSO | 20,20,20,10 | 0,0,0,0 | 0 | 0 | 0,0,0,0 | 0,0,0,0 | 100,100,100,100 | Pictured in Fig. 6 |
| Wild-type | n = 4 | 30 µM Testosterone | 35,27,21,26 | 94,88,80,76 | 85 | 8 | 0,0,0,0 | 0,0,0,0 | 6,12,20,24 | Pictured in Fig. 6 |
| *MZcyp19a1b* $^{uab124}$ | n = 4 | 30 µM Testosterone | 28,26,29,28 | 89,84,75,78 | 82 | 6 | 0,0,0,0 | 0,0,0,0 | 11,16,25,22 | Pictured in Fig. 6 |
| Wild-type | n = 4 | 0.1% DMSO | 12,10,12,14 | 0,0,0,0 | 0 | 0 | 0,0,0,0 | 0,0,0,0 | 100,100,100,100 | Pictured in Fig. 6 |
| heterozygous *esr1a* $^{uab118/+}$ | n = 4 | 0.1% DMSO | 25,24,23,28 | 0,0,0,0 | 0 | 0 | 0,0,0,0 | 0,0,0,0 | 100,100,100,100 | Pictured in Fig. 6 |
| homozygous *esr1a* $^{uab118/-}$ | n = 4 | 0.1% DMSO | 12,12,12,12 | 0,0,0,0 | 0 | 0 | 0,0,0,0 | 0,0,0,0 | 100,100,100,100 | Pictured in Fig. 6 |
| Wild-type | n = 4 | 30 µM Testosterone | 24,26,19,27 | 70,80,78,77 | 76 | 4 | 0,0,0,0 | 0,0,0,0 | 30,20,22,23 | Pictured in Fig. 6 |
| heterozygous *esr1a* $^{uab118/+}$ | n = 4 | 30 µM Testosterone | 44,50,39,45 | 65,86,71,71 | 73 | 9 | 0,0,0,0 | 0,0,0,0 | 35,14,29,29 | Pictured in Fig. 6 |
| homozygous *esr1a* $^{uab118/-}$ | n = 4 | 30 µM Testosterone | 23,22,20,22 | 69,90,75,81 | 79 | 9 | 0,0,0,0 | 0,0,0,0 | 31,10,25,19 | Pictured in Fig. 6 |
| Wild-type | n = 4 | 0.1% DMSO | 10,13,11,14 | 0,0,0,0 | 0 | 0 | 0,0,0,0 | 0,0,0,0 | 100,100,100,100 | Pictured in Fig. 6 |
| heterozygous *esr2a* $^{uab134/+}$ | n = 4 | 0.1% DMSO | 20,25,18,29 | 0,0,0,0 | 0 | 0 | 0,0,0,0 | 0,0,0,0 | 100,100,100,100 | Pictured in Fig. 6 |
| homozygous *esr2a* $^{uab134/-}$ | n = 4 | 0.1% DMSO | 11,12,12,12 | 0,0,0,0 | 0 | 0 | 0,0,0,0 | 0,0,0,0 | 100,100,100,100 | Pictured in Fig. 6 |
| Wild-type | n = 4 | 30 µM Testosterone | 30,30,25,30 | 70,70,84,80 | 76 | 7 | 0,0,0,0 | 0,0,0,0 | 30,30,16,20 | Pictured in Fig. 6 |
| heterozygous *esr2a* $^{uab134/+}$ | n = 4 | 30 µM Testosterone | 52,57,56,67 | 73,80,82,86 | 80 | 5 | 0,0,0,0 | 0,0,0,0 | 27,20,18,14 | Pictured in Fig. 6 |
| homozygous *esr2a* $^{uab134/-}$ | n = 4 | 30 µM Testosterone | 30,39,25,30 | 66,84,84,83 | 79 | 9 | 0,0,0,0 | 0,0,0,0 | 34,16,16,17 | Pictured in Fig. 6 |
| Wild-type | n = 4 | 0.1% DMSO | 11,11,13,10 | 0,0,0,0 | 0 | 0 | 0,0,0,0 | 0,0,0,0 | 100,100,100,100 | Pictured in Fig. 6 |
| heterozygous *esr2b* $^{uab128/+}$ | n = 4 | 0.1% DMSO | 18,22,27,20 | 0,0,0,0 | 0 | 0 | 0,0,0,0 | 0,0,0,0 | 100,100,100,100 | Pictured in Fig. 6 |
| homozygous *esr2b* $^{uab128/-}$ | n = 4 | 0.1% DMSO | 12,12,12,12 | 0,0,0,0 | 0 | 0 | 0,0,0,0 | 0,0,0,0 | 100,100,100,100 | Pictured in Fig. 6 |
| Wild-type | n = 4 | 30 µM Testosterone | 24,30,36,47 | 87,80,88,85 | 85 | 4 | 0,0,0,0 | 0,0,0,0 | 13,20,12,15 | Pictured in Fig. 6 |
| heterozygous *esr2b* $^{uab128/+}$ | n = 4 | 30 µM Testosterone | 76,61,67,80 | 77,77,86,82 | 81 | 4 | 0,0,0,0 | 0,0,0,0 | 23,23,14,18 | Pictured in Fig. 6 |
| homozygous *esr2b* $^{uab128/-}$ | n = 4 | 30 µM Testosterone | 32,26,33,34 | 84,80,84,90 | 85 | 4 | 0,0,0,0 | 0,0,0,0 | 16,20,16,10 | Pictured in Fig. 6 |

**Table 5**. Embryo data accompanying Figure 6. Experiments within horizontal lines were performed together.